SEAFLOOR ELEVATION TRENDS AS ENVIRONMENTAL FEATURES FOR DATA ASSOCIATION IN UNDERWATER SIMULTANEOUS LOCALIZATION AND MAPPING

by

Colin MacKenzie

Submitted in partial fulfilment of the requirements
for the degree of Master of Applied Science

at

Dalhousie University
Halifax, Nova Scotia
October 2015

DEDICATION PAGE

I dedicate this thesis to my parents whose belief in me never wavered.

TABLE OF CONTENTS

LIST OF TABLES

LIST OF FIGURES

ABSTRACT

While critical to the Simultaneous Localization and Mapping (SLAM), process data association is often unreliable, especially so in a noisy, dynamic, underwater environment. This thesis presents a novel approach for data association that enhances underwater SLAM on autonomous underwater vehicles (AUV) using side-scan sonars. It does this by jointly associating the relative position of a landmark to the AUV with the seafloor elevation gradients surrounding the landmark. The local elevation gradients are extracted from the same side-scan sonar images as the landmarks. Seafloor gradients are relatively stable environmental features compared to the much smaller landmarks which can be subject to movement and positional changes over time due to currents and shifting bottom cover. This concept was found to yield correct associations when implemented and validated in post-processing of data using a hardware-in-the-loop AUV simulator and side-scan sonar data from earlier trials. The algorithm has been installed on an IVER3 AUV and in-water trials are validating this concept in a real world setting.

LIST OF ABBREVIATIONS USED

ADCP	Acoustic Doppler Current Profiler
ATD	Automated Target Detection
ATR	Automated Target Recognition
AUV	Autonomous Underwater Vehicle
BPSLAM	Bathymetric distributed Particle SLAM
CDS	Connected Dominating Set
CLSF	Constrained Local Sub Map Filter
CML	Concurrent Localization and Mapping
DPG-SLAM	Dynamic Pose Graph SLAM
DRDC	Defence Research and Development Canada
DOF	Degrees-of-Freedom
DVL	Doppler Velocity Log
EIF	Extended Information Filter
EKF	Extended Kalman Filter
EM	Electromagnetic
GPS	Global Positioning System
ICNN	Individually Compatibility Nearest Neighbour
IMU	Inertial Measurement Unit
INS	Inertial Navigation System
iSAM	incremental Smoothing and Mapping

JCBB	Joint Compatibility Branch and Bound
LMS	Least Mean Squares
MAS	Multi Agent System
MCM	Mine Countermeasures Mission
MOOS	Mission Oriented Operating Suite
MLO	Mine-Like Object
MSIS	Mechanically Scanned Imaging Sonar
NMCM	Naval Mine Countermeasures Mission
NN	Nearest Neighbour
OEM	Original Equipment Manufacturer
PDF	Probability Density Function
RBPF	Rao-Blackwellized Particle Filter
RF	Radio Frequency
ROV	Remote Operated Vehicle
SAM	Smoothing and Mapping
SEIF	Sparse Extended Information Filter
SIFT	Scale Invariant Feature Transform
SLAM	Simultaneous Localization And Mapping
SSS	Side Scan Sonar
SURF	Speeded Up Robust Features
TIFF	Tagged Image File Format

USV	Unmanned Surface Vehicle
UUV	Unmanned Underwater Vehicle
WP	Waypoint

ACKNOWLEDGEMENTS

I would like to acknowledge the support of my friends and family. Thank you to the Mechanical Engineering graduate students for their assistance and advice, specifically Timothy Pohajdak for his help in coding. Thank you to the members of my committee, with special thanks to Dr. Mae Seto, who provided invaluable knowledge, guidance and time.

I would also like to acknowledge the support of The Office of Naval Research (Global), Massachusetts Institute of Technology, Defence R&D Canada, IEEE – Oceans Engineering Society and NSERC.

CHAPTER 1. INTRODUCTION

Robotics are being used in an ever increasing number of roles where they offer distinct advantages over human workers. Robots are not subject to human error, do not become tired or vary their quality of work, and, key for many applications, they can complete tasks that are dangerous without putting humans at risk.

For many applications it is desirable to have robots that require minimal operator input to maximise their efficiency. Often these robots must be able to interpret their current situation and "make a decision" on how to proceed. These situations can range from simple cases requiring a standard logic gate, if false proceed one way if true proceed another, all the way to fully autonomous missions with robots capable of carrying out complex tasks and responding to the dynamic environments they operate in based on in-situ measurements they make (self-driving cars). Autonomy in robotic systems requires the machine to view, and to some extent, understand its environment. Under circumstances where a robot does not have prior knowledge of its environment it can operate by creating a map of its surroundings while simultaneously establishing its own position within that map and its path of travel. This process is termed Simultaneous Localization and Mapping (SLAM) and is considered a fundamental component of true robot autonomy in any environment. Recognition of landmarks is a critical component of SLAM, and is used for obstacle avoidance, as well as determining if the landmark in question is a new object or has been viewed at some previous time during a mission. This matching of landmarks is known as data association. While much of the current SLAM research makes the assumption that data association results will be valid [1] this is not always the case, especially in underwater environments which often have landmarks that are particularly challenging to identify or re-identify if the environment has changed the landmark's appearance.

1.1. MOTIVATION

SLAM can be a component of an autonomous underwater mission whether it be scientific research, search and rescue, marine salvage or military applications. One potential application, Navel Mine Countermeasure Missions (NMCM), is to survey for

underwater mines that pose serious risks to high value assets as well as human lives. Current NMCM practice often utilizes tethered and/or towed vehicles equipped with side-scan sonar to survey for Mine-Like Objects (MLO). The sonar images are processed and manually reviewed by trained operators who determine if the surveyed area is cleared to a sufficient level or has potential MLO's requiring further action. It can be a lengthy and labour intensive process before an area is verified to be clear to an acceptable degree of certainty using tethered or towed vehicles. However, this is slowly changing to using autonomous underwater vehicles (AUV) integrated with side scan sonars and to perform the initial detection of MLOs in the sonar imagery using on-board the AUV.

In contrast the use of AUVs for NMCM potentially offers increased speed, reliability and consistency. To perform these or other missions it would be useful if AUVs could perform accurate SLAM. AUVs have onboard sensors that estimate the vehicle's dead–reckoned position [2], however over time their position can become increasingly inaccurate. The error in a dead reckoned position is directly relative to the duration since the vehicle's last exact known position (GPS at the surface). While the vehicle's position can only be estimated by dead-reckoning, its' position relative to landmarks it sees can be as accurate as the available sensors allow. Landmarks viewed earlier in a mission have a more reliable position within the mapped environment due to the lower cumulated error in the dead-reckoned position. By recognising a landmark as being previously observed, at a time when its location was more certain, the vehicle can update and improve its current estimated position.

Data association becomes important for carrying out autonomous missions in an always challenging underwater environment where SLAM has been chosen as the mapping methodology. Battery life limits the length of time a mission can last and dead-reckoning under water can be complex with the ability to move in six degrees-of-freedom. Further, the high attenuation, low bandwidth, and multi-path response for water to RF or optical energy means that only acoustics can be used for communications. Given that, acoustical communication still has relatively low bandwidth and can be unreliable due to high attenuation, multi-path, and scattering. Side-scan sonar is one of the most common sensors used in underwater survey missions. Its wide swath covers an area and allows the vehicle

to view the same area multiple times in quick succession, if neighboring scans in a lawn mower survey are spaced closer than the sonar swath area. The multiple views of the same area from different perspectives provide opportunities for data association, however features of landmarks viewed with side-scan sonar are aspect dependent. As well, the quality of sonar scaling and resolution is much less than that of visible wavelength camera images above water.

The seafloor can be sparse and largely devoid of unique detail making conventional landmark associations difficult. However, it is rarely perfectly flat, there are usually peaks and valleys that change gradually or rapidly. It is these very environmental features this thesis uses to augment the strength of an association. By matching the direction and magnitude of the seafloor from an identified landmark to another area a unique profile for each target can be created, improving the accuracy and dependability of the data association process.

Since this process does not take into account features specific to the target itself it is meant as a complementary component to a larger data association algorithm, not a replacement. The thesis uses multiple scenarios that are tested for comparison, with targets matched based on both parallel and orthogonal views. Profiles for each target must be unique enough to be differentiated when attempting to associate to other multiple targets located in a near-by area. The in-water testing of this paper's algorithm was completed over an area which offers a fairly sparse environment with distinct landmarks deliberately deployed for this purpose.

1.2. THESIS CONTRIBUTIONS

This thesis examines and validates a hypothesis for a novel method to augment the SLAM data association for an autonomous underwater vehicle (AUV) using side scan sonar to perform naval mine counter-measures survey missions. Potential targets are additionally classified by the gradient of the seafloor around them. Such environmental feature sets do not take details of the landmarks themselves into consideration and can therefore avoid ambiguity issues, like aspect dependence, associated with how landmarks are observed/sensed with side-scan sonar. Contributions of this thesis include:

i. Extracting detailed elevation profiles of the seafloor from the side scan sonar data files normally discarded after the landmarks are extracted. These maps are produced using already available sensor data logged by the AUVs and do not require additional sensors.

ii. Software tools that robustly orients and filters the sonar images currently being generated so that the landmark extraction software does not need to be accessed. The developed software tools also approximates the seafloor's bathymetry, geo-references all identified MLOs and stores a unique feature set of elevation changes for each landmark for potential associations with the others.

iii. A validation of the data association algorithm with in-depth testing of the procedure using the elevation feature sets with a direct comparison against actual sonar data, concluding with a clear algorithm and its validation.

1.3. THESIS ORGANIZATION

This thesis is organized in the following manner:

- Chapter 2: The literature review provides a background of the basic functionality of AUVs and how they navigate pre-planned missions. This is followed by a review of the history of SLAM and its use on AUVs. Then, a more in-depth description of data association and its challenges is provided, including how this thesis intends to improve the data association process. Details on the SLAM algorithm used in this document are also reviewed.

- Chapter 3: Provides a description of the hardware used in these experiments and the setup of how this new process will be integrated into the previous AUV framework.

- Chapter 4: Covers the theory of elevation data creation used in this thesis as a tool for environmental features in data association, as well as the initial results from a simplified version of this process.

- Chapter 5: Develops an algorithm validation to determine the process's idealized evaluation method using only the data outputs already produced by the AUV.
- Chapter 6: Discusses the major conclusions from the thesis and a direction for future research to further develop the concepts.

CHAPTER 2. LITERATURE REVIEW

This review begins by providing a history of the development of SLAM and how it reached its current state. There is a focus on data association and the current challenges with this process before a more in-depth breakdown of the SLAM algorithm used in the research.

2.1. AUTONOMOUS UNDERWATER VEHICLES (AUVS)

Autonomous Underwater Vehicles (AUVs) are used in a variety of applications for research and exploration. Their ability to operate without tethers or communicating with the surface allows them to collect data in areas manned vehicles cannot easily access. The SLAM process would be useful to their operation as positioning through GPS is not an option underwater and SLAM offers a less resource intensive option for these applications. For the purpose of this document we focus on AUVs similar to the IVER 2 and 3 by Ocean Server.

2.1.1. DESIGN

Many AUVs take on the profile of a torpedo for hydrodynamic-efficient movement through water and the IVER 3 (OceanServer, MA) is an example. The AUV has a rear propeller to provide thrust to move it forward and four fins to control its attitudes and altitude/depth [3]. AUVs are normally equipped with acoustic modems for underwater communications and ranging towards positioning and have a wide array of sensor payloads that can be integrated [4], [5]. Additional details on sensor types and functions are discussed in the next section. Figure 1 below shows an IVER2 AUV with a payload sonar.

Figure 1 – OceanServer™ IVER2 [4]

2.1.2. COMMUNICATION

Effective autonomous vehicle communications are critical to abort a mission, provide information on the state of the vehicle, and/or to allow multi-vehicle coordination [6]. Typical communications between autonomous vehicles and their operators tend to require significant bandwidth to achieve the required levels of vehicle control. As previously mentioned the high attenuation rate of signals in water mean wireless RF communications, which can provide large data transfers, are not a viable option. An example of this is electromagnetic (EM) waves which operate at high frequencies (in the MHz). Their absorption rate in the ocean is even higher than in fresh water because of increased electrical conductivity due to the dissolved salts in the water [5].

Anguita et al. [7] explored the concept of using optical communications underwater but found the range limited to less than 100 metres by the large attenuation of light in water. There were additional negative results caused by ambient noise and the need for a clear line of site from transmitter to receiver which cannot be assured underwater given refraction and scattering at optical frequencies.

Acoustical communications are the most commonly used and reliable underwater technology available, although they also have limitations. While acoustics offer an effective range orders of magnitude greater than that possible with optics, their reach is still limited to approximately 5 kilometres, and increasing distance reduces the success rate of data being received. Acoustical communications must also operate at a relatively low frequency, 9 – 13 kHz, to obtain this range [8], [9]. Lower frequency transducers have a disadvantage in that they are physically larger than their high frequency counterparts and have correspondingly lower bandwidth.

Underwater acoustics are often described as having rapidly fading channels with complex sound propagation [10]. One option that has been explored to improve reliability and data transfer rates is to create networks of acoustic modems throughout an environment where AUV's will operate. Unfortunately this is not a realistic option for missions in unknown or unfamiliar areas or missions that require stealth [11].

2.1.3. UNDERWATER NAVIGATION

Remote underwater navigation and positioning are uniquely challenging tasks. Although AUV's are typically equipped with GPS they do not receive updates while submerged underwater as the penetration for RF into water is very small. All wireless underwater communication is complicated by the high attenuation and low bandwidth inherent in underwater acoustics.

2.1.3.1. UNDERWATER DEAD-RECKONING AND POSE

After diving, the vehicle uses dead-reckoning to provide an estimate of its pose and location. It does this by taking a Bayesian approach assuming its current state is affected by its previous state and current motor commands, the Markov assumption [5], [12]. A standard approach to this is to take into consideration the AUVs heading, speed and the time elapsed from one state to the next [13].

The dead reckoning approach for AUVs will always incur error in the estimation made about their position, and this error will compound if not checked or corrected. The longer a mission operates in these conditions the greater the position error becomes [5], [14].

One approach to zero the accumulated position error is to periodically surface the AUV to verify its GPS position. This can be successful [13] but is not ideal in many situations. Surfacing is an inefficient use of time and battery power during a mission (especially, one in deep water) and AUVs may not be able to easily surface if they are underneath ice, performing stealth missions, or missions at very low depths [5].

Sensors can be integrated with the AUVs as payloads and many of these can aid in the vehicle's localization and provide increased accuracy in dead-reckoning [4]. The most common sensors for assisted dead-reckoning are Doppler velocity logs (DVL) which reflect sound waves directly beneath the vehicle to the seafloor to determine the vehicle altitude and speed over ground, and inertial measurement units (IMU), which can record the vehicles unintended movements in six degrees-of-freedom (yaw, pitch, roll, surge, sway, heave). These give the vehicle more precise calculations of velocity and heading. A

more in-depth description of these and other common underwater sensors can be found in Table 1.

2.1.3.2. RANGE EXTRACTION FROM SONAR DATA

Accurately calculating the distance from an AUV to some target, object or feature in its path is useful to navigation [12]. One method to complete this task is through the use of Mechanically Scanned Imaging Sonar (MSIS) [15]. MSIS sensors emit ultra-sonic pulses and in response an echo intensity profile is received. This is not direct range data but the information can be used to calculate distances to specific objects. The highest echo intensity typically corresponds to the distance to the largest object in the beams' path, although basic image filtering techniques such as thresholding the range of pixel intensity fluctuation can help reduce noise from the environment [15].

Information on obstacle size and distance is used in obstacle avoidance as well as localization and mapping functions but MSIS acoustic processing is only one option for providing such information. The DRDC IVER AUVs are equipped with on-board automatic target recognition software (ATR) discussed in more detail in Chapter 3.2. The distance from the AUV to targets is calculated and stored as part of the ATR analysis.

2.1.3.3. STATE ESTIMATION

Knowing that error is present even with assisted dead-reckoning, state estimation is also used as a process to reduce the uncertainty in the current state of a system using known motor commands and sensory inputs. The systems' state is then filtered to improve the state estimation. There are three commonly used versions of state estimation to improve approximations of an AUV's position: the standard Bayes filter, the Kalman filter and the extended Kalman filter (EKF).

2.1.3.4. THE BAYES FILTER

A Bayes filter is a probabilistic method of state estimation where the believed distribution of the vehicle's state is represented by a Probability Density Function (PDF) [12], [16]. Each time sensor data is collected the PDF of the AUV's pose is also updated [5], [17]. The algorithm for a Bayes filter is as in Equation. (1) [5]:

$$bel'(x_t) = \int p(x_t \mid u_t, x_{t-1})\, bel(x_{t-1}) dx_{t-1}$$

$$\boldsymbol{bel(x_t) = vp(z_t \mid x_t)\, bel'(x_t)} \quad (1)$$

Where the prediction model p is a function of x_t, the estimated vehicle state. This algorithm uses the previously believed state $bel(x_{t-1})$, the current sensor inputs z_t and the measurement input u_t and the normalization constant v to calculate the new belief distribution $bel(x_t)$.

2.1.3.5. THE KALMAN FILTER

The Kalman filter is an optimised Bayesian system that makes two key assumptions about the system: that the system is linear and that any noise in the state or measurement is Gaussian. Since AUV navigation does not meet these criteria the Kalman filter is not a practical tool in these circumstances, however it leads to the extended Kalman filter, discussed in the section below, which is a more useful estimation technique.

The Kalman filter uses the mean and covariance of the PDF for the previous state, measurement input, and sensor input for its algorithm ($\mu_{t-1}, \sum_{t-1}, u_t and\ z_t$ respectively) [5]:

$$\bar{\mu}_t = A_t \mu_{t-1} + B_t u_t$$

$$\bar{\Sigma}_t = A_t \Sigma_{t-1} A_t^T + Q_t$$

$$K_t = \bar{\Sigma}_t C_t^T \left(C_t \Sigma' C_t^T + R_t\right)^{-1}$$

Returned values:

$$\boldsymbol{\mu_t = \bar{\mu}_t + K_t(y_t - C_t(\bar{\mu}_t))}; \qquad \boldsymbol{\Sigma_t = (I - K_t C_t)\bar{\Sigma}_t}$$

2.1.3.6. THE EXTENDED KALMAN FILTER

As introduced in the previous section, the extended Kalman filter is used to linearize non-linear systems around a 1st order Taylor series approximation. This technique has proven to have some success as a state estimation tool for underwater vehicles [5]. The EKF uses the same inputs as the Kalman filter, ($\mu_{t-1}, \sum_{t-1}, u_t and\ z_t$), while also including Q_t and R_t, the normal process and measurement noise distributions, respectively. The

primary noise contributor in an underwater dead-reckoning environment is drift due to currents. This and other noise factors are included in the EKF and the resulting estimations are weighted to the least uncertain values giving the estimation a higher accuracy [5], [17]. The algorithm for an extended Kalman filter is [5]:

$$\bar{\mu}_t = f(\mu_{t-1}, \mathrm{u_t}, 0)$$

$$\bar{\Sigma}_\mathrm{t} = A_t \Sigma_{\mathrm{t}-1} {A_t}^T + W_t Q_{t-1} W_t^T$$

$$K_t = \bar{\Sigma}_\mathrm{t} {H_t}^T \left(H_t \bar{\Sigma}_\mathrm{t} {H_t}^T + V_t R_t V_t^T\right)^{-1}$$

Returned values:

$$\boldsymbol{\mu_t} = \bar{\boldsymbol{\mu}}_\boldsymbol{t} + \boldsymbol{K_t}\left(\mathbf{z_t} - \mathbf{h}(\bar{\boldsymbol{\mu}}_\boldsymbol{t}, \mathbf{0})\right); \qquad \boldsymbol{\Sigma_t} = (\mathbf{I} - \boldsymbol{K_t H_t})\bar{\boldsymbol{\Sigma}}_\mathbf{t}$$

2.1.4. COMMON AUV SENSORS

Table 1 – Underwater non-acoustic sensors commonly integrated into AUVs [15]

Type	Name	Information returned	Successful applications	Weakness
Non-acoustic	magnetic compass	heading	path planning	susceptible to environmental error (ships)
	mechanical gyroscope	angular heading	IMUs	-
	Inertial Measurement Unit (IMU)	acceleration/ rotation in three directions within an internal reference frame	determining pose and heading, dead reckoning	compounding error grows with mission duration
	Global Positioning System (GPS)	accurate location, longitude and latitude	localization	not functional underwater
	pressure Sensor	depth	depth keeping	-

Table 2 – Underwater acoustic sensors commonly fixed to AUVs [15]

Type	Name	Information returned	Successful applications	Weakness
Acoustic	Doppler Velocity Log (DVL)	velocity over seabed and altitude	navigation	-
	multi-beam/bathymetric	depth profile	seabed feature profile	resolution α $^{1}/_{\text{frequency}}$
	acoustic Doppler current profiler	current profile	increased navigation accuracy	resolution α $^{1}/_{\text{frequency}}$
	sub-bottom profiler	determine contents of the seabed	finding buried targets	-
	forward-looking sonar	forward looking feature profile	obstacle avoidance, range finding	-
	side scan sonar	2D image from side viewed intensity profiles	feature and target detection within a wide array	resolution α $^{1}/_{\text{frequency}}$

2.2. SIMULTANEOUS LOCALIZATION AND MAPPING (SLAM)

To consider vehicles truly autonomous they must accurately determine their location without external assists. This usually entails identifying significant features and structures in their surrounding environment in order to add them to the internal map they are building, and being able to localize themselves within that map. In some vehicles this is achieved directly using the GPS to determine location, but there are a number of situations where

this may not be possible. The GPS receiver can only retrieve information on its own position and not obstacles, terrain, or moving objects within the vehicle's environment. In situations where communications are poor because of being indoors, underwater, in inclement weather, or in areas where signals are purposely blocked, the GPS may not be accessible [11]. Simultaneous Localization and Mapping (SLAM), also referred to as Concurrent Mapping and Localization (CML) is a one approach to vehicle autonomous navigation.

2.2.1. BACKGROUND

Localization and mapping for robotic vehicles was originally approached as two separate tasks. However in the late 1980s and early 1990's it was determined that each information set could aid the other in reducing their overall effort and error [2].

All robots navigate their environment through data they collect from attached sensors. SLAM is a technique used by vehicles to build a map of their environment through processing the data (into information) provided by these sensors and to track their own locations within that map. The most basic premise is the ability to extract feature information about landmarks from the surrounding environment. Landmarks that can be successfully incorporated into the SLAM process include, but are not limited to, corners, rocks, terrain features, anchor scars, elevation changes etc. [2], [18]. Objects identified as landmarks are recorded based on their unique structure, and their position is incorporated into the vehicle's map of its environment.

A Doppler velocity log (DVL) and inertial measurement unit (IMU) are standard sensors that allow the vehicle to estimate its change in pose over time as a consequence of navigating with these sensors. While this more advanced form of dead-reckoning yields a reasonable approximation of the vehicle's location, placement errors caused by uneven winds/currents, terrain, motor slipping, operating within a moving fluid, and calibration error are unavoidable. These errors if unchecked will grow the longer the vehicle operates, leading to potentially large position errors. To correct these errors periodic "closing the loop" for the map becomes a necessary part of the navigation process [5], [17]. Ideally when a vehicle views a set of features that it recognizes as a previously observed landmark,

as opposed to a new unknown one, it updates its estimated pose to its known pose from its position relative to this landmark. Its path from the last viewed known landmark is then corrected to account for this estimation error.

2.2.2. EVOLUTION OF SLAM

As SLAM research continues to evolve each new approach yielded improved results in some areas, but invariably shortcomings remained, which inspired the next algorithm dynamic SLAM. This section briefly outlines the primary components that contribute to the current SLAM algorithm.

2.2.2.1. PROBABILISTIC SLAM

A major advance in SLAM arrived with the concept of using probabilistic reasoning to determine the vehicle posterior given the prior knowledge of landmarks [17]. This is represented as in Equation.(2):

$$p(x_{1:k}, m | z_{1:k}, u_{1:k}). \tag{2}$$

Where *x* is the vehicle`s pose, *m* is the map, *z* is the measurements, and *u* represents the vehicle's controls, all at time, *t.* Equation 1 provides the PDF of *x* and *m* given that the information of *z* and *t* are known. This approach is a form of Bayesian probability where the current state is assumed to be only affected by the previous state, and current control inputs and measurements [12], [17]. The vehicle's pose is never definitively known, but the formed probability density function over all possible positions shows where it is most likely to be located, with this position becoming more likely the more often landmarks are correctly recognized and associated. Figure 2 shows a series of several iterative steps performing probabilistic Bayesian SLAM. [2]

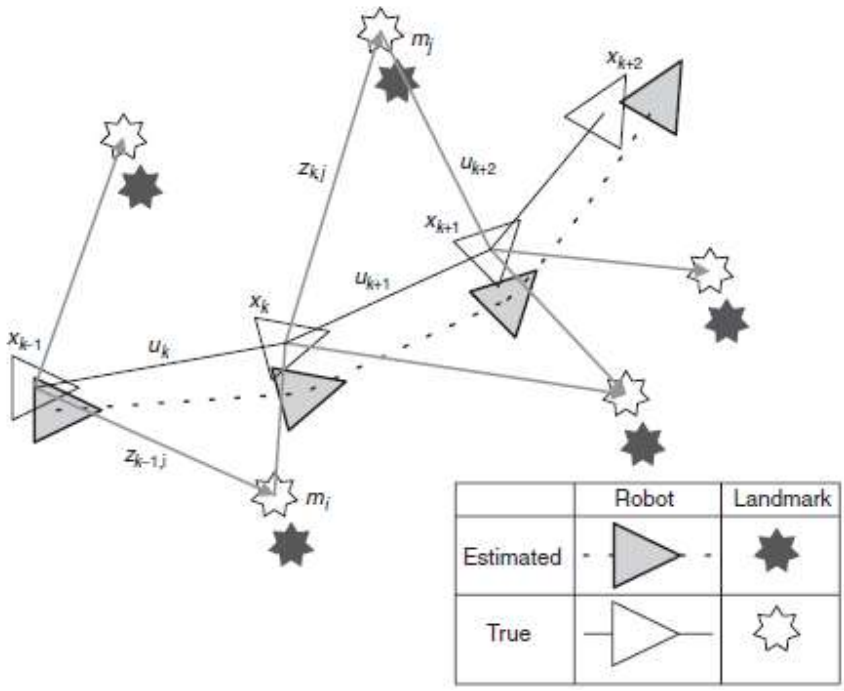

Figure 2 – Vehicle pose at several stages with links to landmarks [2]

2.2.2.2. EKF – SLAM

The use of a state estimator, such as a Kalman filter, reduces the uncertainty associated with each measurement in the SLAM process. In practice these systems are not linear and therefore an extended Kalman filter is required [19]. A more in depth discussion on EKFs is found in Chapter 2.1.3.6.

$$p(x_k|x_{k-1}, u_k) \leftrightarrow x_k = f(x_{k-1}, u_k) + w_k \quad (3)$$

In this Equation (3), f(·) represents the vehicle's motion model and w_k represents the environmental noise. The primary complication in this process was computational time. The first successful case of underwater EKF -SLAM was achieved by Paul Newman in 1999 [2]. Many real world environments contain dozens (sometimes hundreds or more) of usable geographic features and this number can grow rapidly with increased environment size. Simple EKF-SLAM updates the covariance matrix for each new landmark observed, which has a significant effect on the computational complexity of the system. In fact there is a quadratic relationship between required processing time and the number of landmarks observed [2], [17], [20] which prevents real time SLAM in most situations. While there are

a number of ideas on how best to mitigate this problem, the most researched options are map segmentation, the Rao-Blackwellized Particle Filter (RBPF), Sparse Extended Information Filter (SEIF), and Bathymetric profile SLAM.

2.2.2.3. MAP SEGMENTATION

A conceptually basic approach to reducing map complexity is to break the global map into a series of smaller sub maps, each with a more manageable number of features to process [2], [20]. These sub maps are fixed to a global coordinate system, while relative transforms must be tracked that relate each sub map to the others. This can be done using partially overlapping sub maps that can be merged by recognizing overlapping features in adjacent maps [21]. Another approach uses a hierarchical system that focuses on updating one small section at a time for incorporation into a global map [22]. An example of this is the Constrained Local Sub map Filter (CLSF) [23], [24].

While these methods produce more robust results than standard EKF-SLAM, they still do not solve the fundamental problem with this method since map complexity and process time quickly becomes unwieldy [2].

2.2.2.4. FASTSLAM

FastSLAM is also an attempt to improve efficiency of the SLAM process. FastSLAM was originally introduced by Montemerlo et al. [25] in 2002 and was the first time the SLAM problem was approached without the simplifying assumption the system was linear and Gaussian. Particle filters are inherently too computationally complex to be robust for large areas. The Rao-Blackwellization algorithm is used to reduce this complexity to a more manageable state [2].

This is done by determining the probability distribution of the vehicle's total trajectory $\boldsymbol{X}_k$ instead of for each individual state x_k. This gives linear complexity to the system for each additional node rather than the quadratic complexity of the EKF-SLAM algorithms. The EKF-SLAM complexity is shown in Equation 3 as $\sim O(K^2)$ and becomes $\sim O(Mlog(K))$, where K is the number of landmarks observed.

The PDF is then determined by:

$$P(\boldsymbol{X}_{0:k}, \boldsymbol{m}|\boldsymbol{Z}_{0:k}, \boldsymbol{U}_{0:k}, \boldsymbol{x}_0) = P(\boldsymbol{m}|\boldsymbol{X}_{0:k}, \boldsymbol{Z}_{0:k})P(\boldsymbol{X}_{0:K}|\boldsymbol{U}_{0:K}, \boldsymbol{x}_0) \quad (4)$$

This SLAM algorithm has shown bounded error results in missions with up to 50, 000 distinct landmarks [17].

2.2.2.5. SPARSE EXTENDED INFORMATION FILTERS

Sparse extended information refers to an unstructured storing of landmark data as it is observed [20], [26]. The SEIF improves computational efficiency by only focussing on landmarks that are directly adjacent to the vehicle or "active" as shown in the far right of Figure 3 [17].

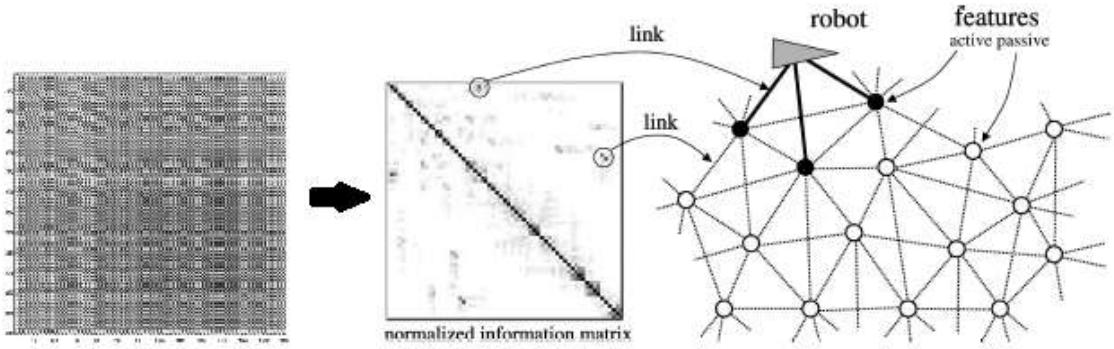

Figure 3 – Covariance matrix EKF-SLAM vs SEIF [17]

The far left image shows a covariance matrix from a standard EKF-SLAM algorithm where the darker nodes indicates a strong correlation between the landmarks. The right section of the image shows the matrix sparsely maintained by the SEIF algorithm avoiding recalculating the unchanging aspects of the matrix. This allows for a much less complex, more robust process.

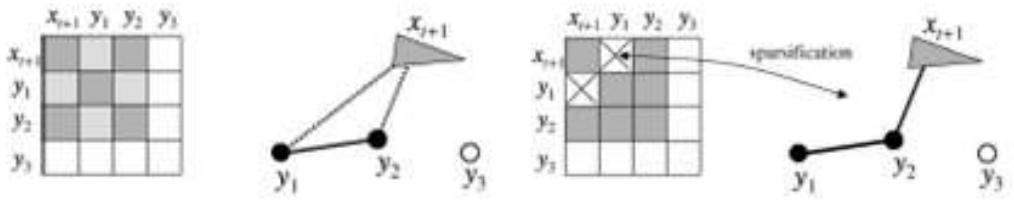

Figure 4 – Sparsification, passive lanmarks removed from covariance matrix [17]

Figure 4 from [17] shows the "sparsification" process zoomed in, where the vehicle's connection to landmark "y_1" is dropped as superfluous, so that when the vehicle updates its pose it only updates the currently "active" landmarks. This algorithm has proven to be successful at producing SLAM results with bounded error even in environments containing a large number of landmarks [17], [26].

2.2.2.6. BATHYMETRIC SLAM

SLAM can be unreliable in environments where distinguishable landmarks are scarce. This is a common issue in underwater SLAM where the seabed can be primarily covered with sediment and landmarks can be difficult to distinguish. The depth profile of the seabed however can vary significantly and it has been suggested that building a bathymetric map using elevation changes as features may be more reliable in certain situations [27]. This technique is referred to as Bathymetric distributed Particle SLAM (BPSLAM) and it has produced successful results profiling the seabed using tow dimensional depth maps. Figure 5 shows a multi-beam bathymetric profile of Halifax's Bedford Basin. This image shows an example of the resolution achievable with this type of sensor.

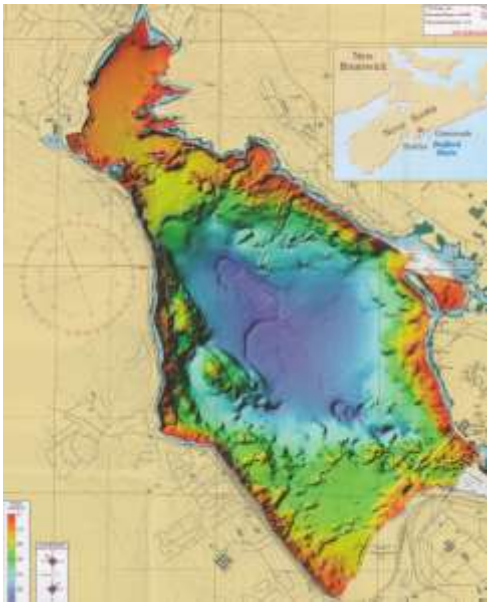

Figure 5 – Bathymetric sonar data, Bedford Basin [65]

2.2.2.7. GRAPH SLAM

A graphical representation of the SLAM problem, Graph SLAM, has 2 types of values represented; motions, that show the vehicles changes in pose from one point to the next and measurements (edges between the poses), that show Euclidean distance from each pose to features within the environment observed from that point. The edges can show measurements between the vehicle poses and to landmarks, and each edge can be thought of as a negative log likelihood of the motion model [28]. These measurement and motion constraints are organized in a sparse information matrix and the graph SLAM function,

which when minimized indicates the most likely path the vehicle travelled and most likely map of the environment.

2.2.2.8. OTHER AREAS OF RESEARCH IN SLAM

There is on-going research on numerous aspects of SLAM aimed at improving both aerial and underwater vehicle performance. Samples of these studies include:

Dissanayake et al. [29] provided an overview of algorithms associated with successful SLAM results (ie. EKF SLAM, FastSLAM), and described some of the most mainstream areas of current research including Smoothing and Mapping (SAM).

Casarrubias-Vargas et al. [30] used machine learning techniques to train a vehicle to find specific landmark types using an EKF-SLAM based system.

Other research focused on improved EKF systems that include robocentric map joining [31]; the use of scale-invariant feature transforms (SIFT) for landmark positioning [32]; and using MSIS data to store state vector information on the vehicle's movements. The key difference with this work is the body centered reference frame which was internal to the vehicle instead of a world reference frame [33].

2.2.2.9. MULTI – VEHICLE SLAM

Up to this point only single vehicle SLAM missions have been discussed. This makes sense as the purpose of SLAM is to allow an autonomous vehicle to operate without external assists. However, there can be significant improvements to SLAM and the abilities of autonomous vehicles through multiple autonomous systems collaborating towards a common goal. Research on numerous aspects of improving collaborative multi-agent systems (MAS) both in air and underwater is being conducted to improve the overall success of autonomous missions.

Operations completed by autonomous vehicles are often limited in difficulty because of the size and intricacy of the environment they manoeuvre though and the resource demands of the computational tasks required. This constraint is often directly linked to limitations associated with the vehicle's battery life, an AUV can only map an area of a certain size before it needs to recharge. This leads to a constant search in vehicle

development for the largest energy density source available to increase the vehicle's endurance and thus the scope of tasks it can perform.

Ideally, the use of cooperative autonomous systems is a tactical way of extending the abilities of an autonomous vehicle. Many researchers, including Sathyanath et al. [34], modelled their systems to replicate the behaviour of biological systems that already accomplish the collaborative tasks vehicles want to emulate. Larger areas can be mapped when multiple vehicles cover different sections of the environment [35], [36]. For small scale missions there are still benefits in time sensitive situations where a single vehicle could complete the job, but not within the time available. As well, another vehicle may have a different resolute or range on its payload sensors which are appropriate for other reasons. There are many examples of multiple vehicles performing the same tasks within a mission, but that is not the only potential advantage to MAS. Each vehicle can be programmed to carry out specific functions while equipped with unique sensors and tasks. Unmanned surface vehicles (USV) could potentially act as communications and navigations points between AUVs, using acoustic modems, and other vehicles operating above the water, using wireless RF signals. USV's can act as platforms for docking and recharging UAV's allowing them to extend their range away from operators. In mine counter measure (MCM) missions selected AUV's can be programmed to perform SLAM and target recognition of mine-like objects (MLO) using side scan sonar with a wide swath, while other AUV's gain higher resolution sensor data of the potential MLO's to increase the certainty of their identification [37].

Another significant potential advantage to MAS is based on landmark locations and features being passed between vehicles, allowing them to locate themselves in areas they had not mapped themselves. This would be a major step forward over single vehicle SLAM where a vehicle must map its environment before it can locate itself [38].

While the potential benefits of MAS are significant to advancing autonomous vehicle SLAM and other areas of research it is an extremely challenging field. The more vehicles that you add to an operation the more you increase the support ship overhead and operational costs, as well as the risk of vehicle loss if recovery is not possible. Unrecovered vehicles are a necessary consideration with any UAV or AUV operation since they are

typically used in situations where manned recovery is not an option or is not feasible for other reasons (extreme weather, mission has changed, threats in the area, etc.).

Communications are critical for any successful multi-vehicle operation. This is particularly difficult for underwater vehicles for the reasons discussed previously. While simulations of underwater SLAM with multiple collaborative vehicles have been successful, their performance under real world conditions has been problematic. This is largely due to the high data transfer rates used, while possible for the modem to output, have a high failure rate under real world conditions [39].

In multi-vehicle SLAM operations, identifying the overlapping areas within each vehicle's map is critical to being able to merge the parts into a global map of the environment [37]. The vehicles' individual maps must be oriented and scaled so that they can be properly merged and georeferenced. This is done by the recognition of identifiable features within the recorded landmarks. There is potential in these situations to have false positives for overlapping map spaces. An example of this is discussed by Thrun et al. [17] using a building with several floors each having the same layout. For this reason it is not just important to recognize matching features within an environment, but also which features are distinct. This variation could include extra or missing landmarks, or landmarks oriented in different ways. Only overlapping sections containing matching features, without significant missing landmarks, are determined to be the same space. Once the maps have been oriented and scaled and overlapping sections identified, the online location of each vehicle and its position relative to the others, can be accurately estimated [17].

As research in underwater vehicle SLAM grows MAS operations are the logical progression towards more efficient and reliable missions. However, substantial improvements in underwater communications will be necessary to make significant advancements in this field. MAS research can be expected to continue to progress as the cost of autonomous vehicles and energy storage systems decrease.

2.2.3. POSE GRAPH SLAM

Unlike the filtering methods of SLAM (Kalman and particle filters) Pose Graph SLAM is a smoothing approach that attempts to estimate the total trajectory of the vehicle

using all available measurements. The vehicle trajectory is represented graphically by a series of nodes and edges, as seen in Figure 6. Each node represents the pose of the vehicle or a landmark while the edges represent the constraints between the two nodes as viewed by the sensors. As with most smoothing algorithms, PG-SLAM uses a least means square (LMS) approach to minimise the error of the vehicle trajectory over the entire trajectory.

2.3. DATA ASSOCIATION

Data association is a primary component of the SLAM process. It refers to situations where new landmark features are compared and associated with landmarks already existing within the SLAM produced map [5], [40]. While this is critical for localization in autonomous robotics, it is currently an unreliable process needing significant improvement to achieve more reliable SLAM missions. A primary focus of improving data association is how to best deal with environmental noise. Noise within the environment can distort a landmark's feature data, but may not be present while viewing the same landmark at a different time or from a different aspect. This can lead to a feature not being recognized as the same previously observed landmark in that same location.

The vehicle constantly calculates its path using dead-reckoning. This information is logged while sensory data, and its processing, is used to define landmarks and their locations by means of various associated features. Connections are created that link the pose of the vehicle to the viewed landmark locations. If a specific landmark is observed again the vehicle's position can be updated from its current calculated state to a truer position. Several feature identification algorithms have been developed to assist removing errors associating landmarks based on orientation and scale. The two most common processes are Scale Invariant Feature Transform (SIFT) and Speeded Up Robust Features (SURF) and these products have led to improved robotic performance in some cases [41].

The most commonly used data association algorithms are nearest neighbour (NN), individual compatibility nearest neighbour (ICNN) and joint compatibility branch and bound (JCBB).

NN requires fairly low computational expenditure but can be susceptible to incorrect associations, matching a set of landmarks using the minimal statistical distance between two targets whose positions are represented by PDFs [42].

ICNN offers a slight improvement on this, taking the Mahalanobis distance (the distance from a point to a distribution) between the two landmarks which, as the name suggests, are evaluated for compatibility separately. These two methods are most likely to incur false associations in an area that contains a cluster of closely placed targets where small inaccuracies in the dead-reckoning estimations can have a larger impact.

JCBB is more computationally intensive but offers increased reliability to NN or ICNN. Taking into account not only the distances of each landmark being compared to each other but also the neighboring landmarks (and their groupings), a branch and bound series determines the best cumulative fit [43]. This allows for the filtering out of false associations which may have yielded close associations without being the correct match.

A comparison of these data association methods are shown in Figure 6 [44].

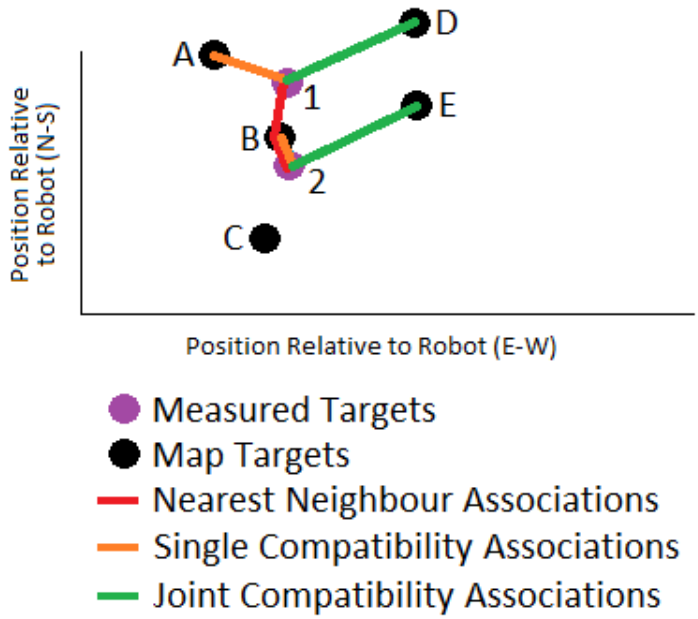

Figure 6 – Comparison of the three most common data association algorithms [44]

Chen et al. [45] have shown improved results using a hybrid form of ICNN and JCBB. Gil et al. [46], used a sparse SIFT with a rejection protocol that only considered features that appeared stable from varying views, to reduce the likelihood of noise distortion. Also using SIFT Xiao-hua et al. [47] examined the minimum Connected Dominating Set (CDS) between the current sensor view and previous sensor views, considering the smallest set of matching features between two landmarks during the comparison. Kosuru et al. [48] compiled feature sets into polygonal shapes to properly associate one set from another.

CHAPTER 3. SYSTEM DESCRIPTION

This section outlines the features of the IVER vehicles used in testing this thesis, including their hardware, SLAM algorithm, data association methods, and how elevation maps are incorporated into the hierarchy.

3.1. HARDWARE OVERVIEW

The IVER 3 (Figure 7) autonomous underwater vehicle is integrated with a MarineSonics HDS (900/1800 kHz) side-scan sonar as the payload sensor as well as a T16 Kearfott INS [49].

Figure 7 – MarineSonics IVER3 AUV [4]

The AUV has two on-board computers (Intel 1.6 GHz processors). The computers referred to as the front seat, or Original Equipment Manfacturer (OEM), and the back seat, or payload computer. The backseat, runs as the vehicle's "autonomous brain" while the front seat controls the misson's navigation and onboard sensors (including DVL, range sensor, depth sensor and compass) [49]. Communications between the OEM and payload computers are shown in Figure 8.

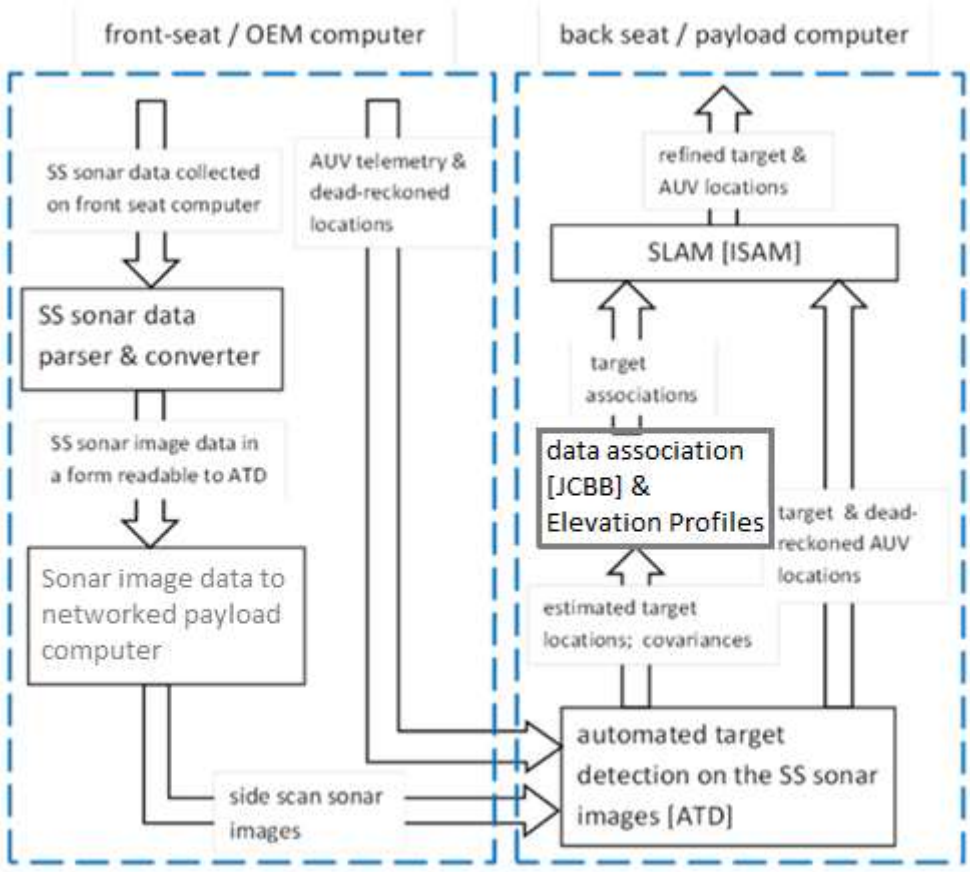

Figure 8 – IVER3 AUV front seat and back seat information flow. IVER3 set up is similar, but with the two computers networked together [44]

Figure 8 shows the OEM manages mission waypoint following, and the collection of side scan sensor and navigation data. Sonar data and dead–reckoned position estimates are passed to the payload computer and are first processed through the ATR (of which the Automated Target Detection ATD is one component). The ATR outputs the targets' estimated locations and covariances (which includes correlating the targets' positions to one another and to the vehicle's) to the SLAM engine [44]. The SLAM algorithm incremental Smoothing and Mapping (iSAM) and ATR are discussed further in sections 3.3.1. and 3.2. respectively. Running as part of SLAM the data association attempts to match landmarks as it observes them in the side scan sonar imagery. It then returns this information to the main SLAM system which then updates its current and prior positions. In the case of NMCM a change to the mission path could be implemented to survey an area

where an MLO was previously observed to re-acquire and confirm the existence and location of the landmark and decide on further prosecution.

3.2. AUTOMATED TARGET RECOGNITION

DRDC IVERs are equipped with a DRDC proprietary target detection software, Automated Target Recognition (ATR) which can identify MLOs from side-scan sonar data [50]. While specifics on the ATR functionality are outside the scope of this thesis, it operates using two major filters speckle, matched. The speckle filter, a simplified approach, operates by scanning the sonar images for clusters of drastic changes in light intensity that could indicate a target sitting above the seafloor and casting a shadow. The speckle filter has a likelihood to have false detections and is more dependent on the quality of sonar data, the sparsity of the environment, and the threshold settings applied at the start of the mission. The matched filter attempts to match the distinct size and geometry of viewed objects based on a comprehensive stored database of MLOs at given ranges and aspects. The matched filter is more resistant to false positives than the speckle filter but still has the potential for false negatives. Other forms of target detection for side scan sonar SLAM used on IVER 3 Vehicles at DRDC similar to the match filter are described in [50]-[53].

Most SLAM algorithms discussed to this point have focused on Bayesian filter SLAM methodologies. Another, more efficient, option is smoothing algorithms such as incremental smoothing and mapping (iSAM) [54]. This algorithm was developed by MITs CSAIL with the underwater environment in mind and is the SLAM algorithm used by DRDC Atlantic.

3.2.1. INCREMENTAL SMOOTHING AND MAPPING (ISAM)

Similar to Graph SLAM [28], [55], iSAM tracks the vehicle's trajectory over the entire mission and maintains a sparse QR information matrix. The structure of this matrix, being an orthogonal matrix Q and a upper triangular matrix R, allows it to be back-solved efficiently providing substantial savings in computational effort. Searching for the maximum likelihood, or minimum error, of the total AUV trajectory results in a smoothing (improved) estimation at each time step making it possible to implement on-line. A smoothing SLAM method such as this can remove previously false estimations. iSAM runs

on the basis of a pose graph model, with the most up to date versions also taking into account the possibility of environmental features not being stationary over time (Dynamic PG-SLAM). Pose Graph SLAM and Dynamic Pose Graph SLAM are described in more detail in the next section.

3.2.2. Dynamic Pose Graph SLAM and Incremental Smoothing and Mapping

Dynamic Pose Graph SLAM (DPG-SLAM) utilizes an incremental Smoothing And Mapping iSAM algorithm (developed by CSAIL of MIT) for the vehicle's state estimation [56]. The information that relates each pose, landmark and measurement is stored in an information matrix. This square root matrix is spare and triangular so it can be back solved, reducing the computational cost that occurs in filtering based SLAM algorithms. One of the primary advantages of the iSAM process is that it can evaluate the vehicle's entire path at each new time step searching, allowing for correction of previously incorrect vehicle or landmark positions.

Real world environments are subject to change over time. In NMCM missions it is common for the same area to be surveyed multiple times over a long period. The ability to track changes that can occur in a dynamic underwater environment, or when a target may have been added to an area, while still maintaining an accurate global map is crucial and DGP-SALM is a leading method to handle dynamic environments.

CHAPTER 4. ELEVATION DATA AS ENVIRONMENTAL FEATURES FOR DATA ASSOCIATION

This chapter describes the theory used to extract environmental elevation data from side scan sonar imagery and evaluate it as part of the data association process. The procedure's initial results are discussed to verify the process's potential and future research.

4.1. THEORY

This section reviews the background theory upon which this thesis is based describing why this data was used, how it was calculated, and how it was applied in the data association.

4.1.1. ENVIRONMENTAL FEATURE SETS

While data association has become reasonably reliable above water where cameras and other available sensors can create detailed imagery of the environment and its landmarks, it remains a significant challenge underwater. There, landmarks can be sparse and ill defined. Many standard target recognition processes such as Scale Invariant Feature Transform (SIFT) [57], [58] and Speeded Up Robust Features (SURF) [59] do not perform well on with aspect dependent sonar data like SSS images. Similar underwater targets can appear non-uniformly varied in size and structure depending on the vehicle's relative position and dynamics at the time they were observed. The subsea environment has great potential for shifting and changing over time from the natural flow of currents. It was decided that one method to improve data association in this setting could be to use the more enduring aspects of the environment around the target. The hypothesis behind this thesis is that topographical aspects of the seafloor may provide enough detail to identify a target using only minimal details of the target itself, outside of its relative position to the AUV. Extracting an estimated bathymetry of the sea floor from SSS has been examined in [2], [60]-[63].This is intended for use in parallel with the JCBB algorithm (discussed earlier), as an additional item to jointly associate a target against, in addition to associations already made through a traditional analysis of the side scan sonar data.

4.1.2. ESTIMATED BATHYMETRY OF THE SEAFLOOR

In order to incorporate the seafloor profile into the SLAM data association the AUV must collect a data on this data during the mission. This can be done in several different ways. One option is to use a bathymetric sonar in addition to the AUV's side-scan sonar. However the added complexity, cost and additional power consumption this would require makes this option less appealing. Alternatively, data already generated by the side-scan sonar can be used to produce an estimated bathymetric representation of the seafloor. This can be done by combining the intensity values in the TIFF images generated for each mission leg and information from the log data files already stored as part of a standard mission.

The values in the generated intensity map (inverse bathymetry) represent the vertical distance (altitude) from the AUV to the seabed at each pixel location and therefore show an inverted profile of the seafloor relative to the AUV. This information can be combined with the recorded depth of the vehicle, also stored in the standard log files, to create a reasonable estimate of each location's true depth.

The altitude at each pixel is calculated by first assuming a Lambertian reflectance model for the seafloor that assumes all locations scatter energy uniformly. The TIFF images are a series of intensity values at each pixel location. This model defines the intensity of values I, as being represented by a relationship of the sonar's beam intensity profile Φ, the location's reflectivity R, and altitude Z as shown in Equation 5.

$$I(x,y) = -K\Phi(x,y)R(x,y) \cdot \frac{Z(x,y) - x \cdot \frac{\partial Z}{\partial x}(x,y)}{\sqrt{x^2 + Z^2(x,y)} \cdot \sqrt{(\frac{\partial Z}{\partial x}(x,y))^2 + (\frac{\partial Z}{\partial y}(x,y))^2 + 1}} \quad (5)$$

The K value is a normalization constant, y represents the distance in the direction of the vehicle heading, and x the distance orthogonal to that heading either on the port or starboard side of the vehicle. The Z map (altitude) was initialized to the altitude of the vehicle at the time of each ping for all pixels along the row of x values. The reflectance map was initialized to values of 0.9 as per [61] and Φ was given the same initial values as I averaged over each angle α, where α is the beam angle to the point of reflection from the

normal *x* as shown in Figure 9. Using a Least Mean Square (LMS) regression a local minimum error for the intensity map was calculated with gradient descent. The most updated version of the *Z* map was then used to represent the inverse bathymetry of the seafloor.

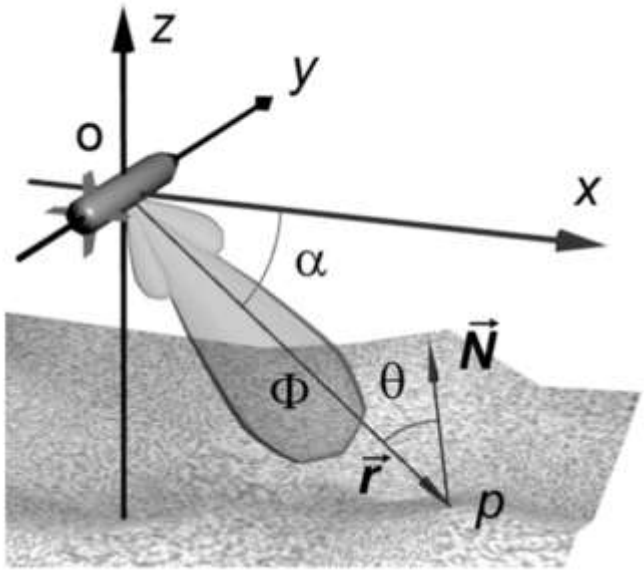

Figure 9 – AUV reference frame for bathymetric estimation [64]

4.1.3. TIFF IMAGE PREPARATION AND NADIR IDENTIFICATION

Generating an accurate view of the bathymetry is limited by the quality of available sensor data, primarily the accuracy of the TIFF image, which must realistically represent the scanned environment. Currently, DRDC IVER AUV's use ATR software to generate the log data files and unscaled images, as well as a scaled (brightened) version of the images. The unscaled images are so dark that that it is difficult to extract useful information from them, or even view landmarks within them. Scaled images offer more detail but can be over brightened, causing many areas to be washed out hiding critical information. Figure 10a and b show unscaled and scaled versions of the same image respectively.

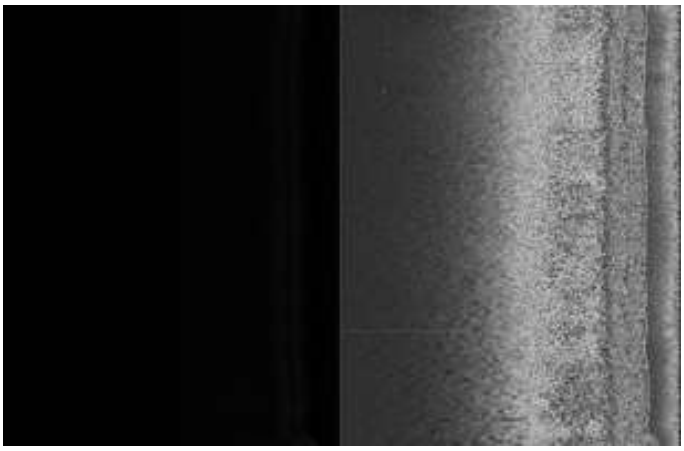

a. b.

Figure 10 – (a) shows the unscaled original image and (b) shows the scaled. Neither are useful for accurate bathymetric estimation

Some scaling issues arise in the image's transition from the area directly below the AUV to the first return from the sonar, which shows a drastic jump in intensity. Side-scan sonar offers wide area coverage but cannot view the ground directly below the AUV (the blind spot). This unseen area appears in the sonar images as a black band known as the nadir, seen in Figure 11.

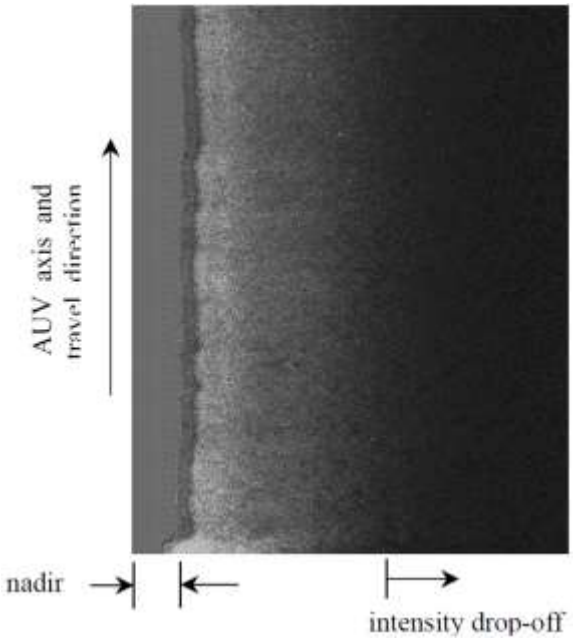

Figure 11 – Standard side-scan sonar image (ATR scaling, from IVER3)

The nadir is misinterpreted by the inverse bathymetry calculations. It views the transition from the dark nadir to the bright first returned sonar value as a large jump in altitude. To compensate for this error a separate set of scaled images were generated by an additional software using the unscaled images from the ATR. The data logs were first used to identify and remove the nadir's dark band before scaling the image brightness to produce a more representative distribution. The nadir was identified using the geometry of the sonar beam shown below from [64] and in Figure 14.

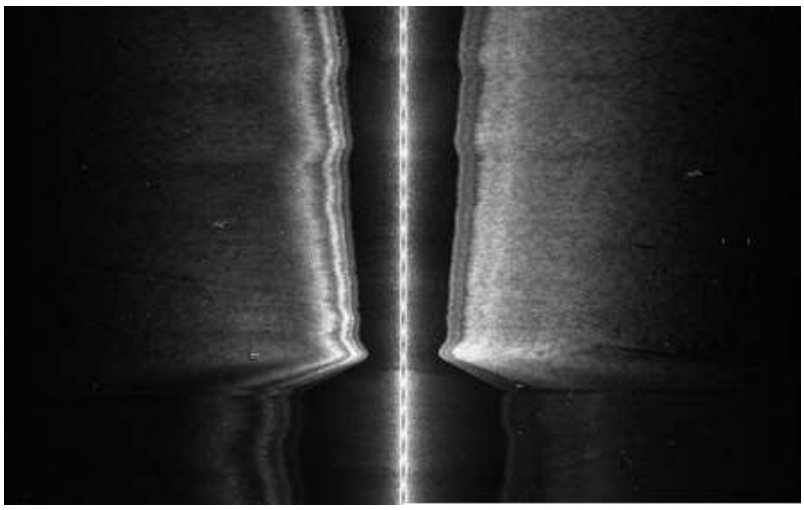

Figure 12 – Port and starboard SSS image

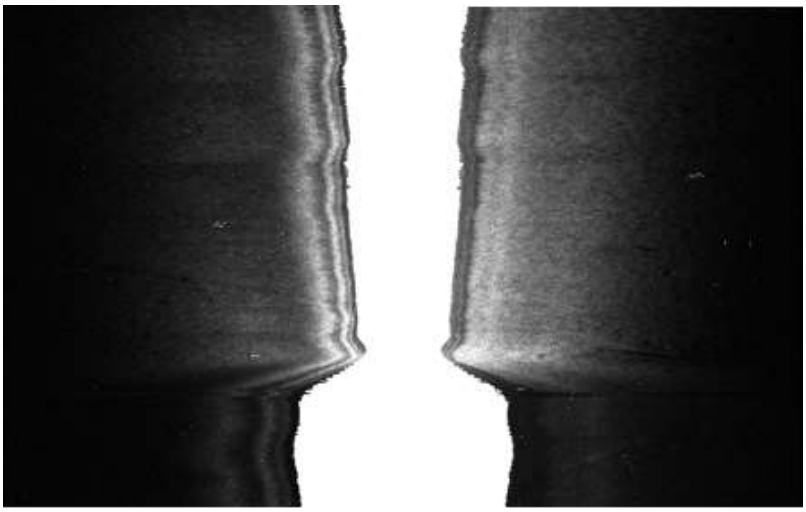

Figure 13 – Same SSS image from Figure 12 with the nadir removed

The nadir's size and shape fluctuates, within the SSS image, with changes in the AUV's altitude, roll, and pitch. Since the geometry of the sonar's coverage is known, the

location of the last pixel of the nadir, or first sonar return from the seafloor can be identified. Figure 14 shows the outline of the vehicle geometry where $\left(\theta + \frac{\propto}{2}\right)$ is the angle from the AUV's horizontal axis to the end of the nadir.

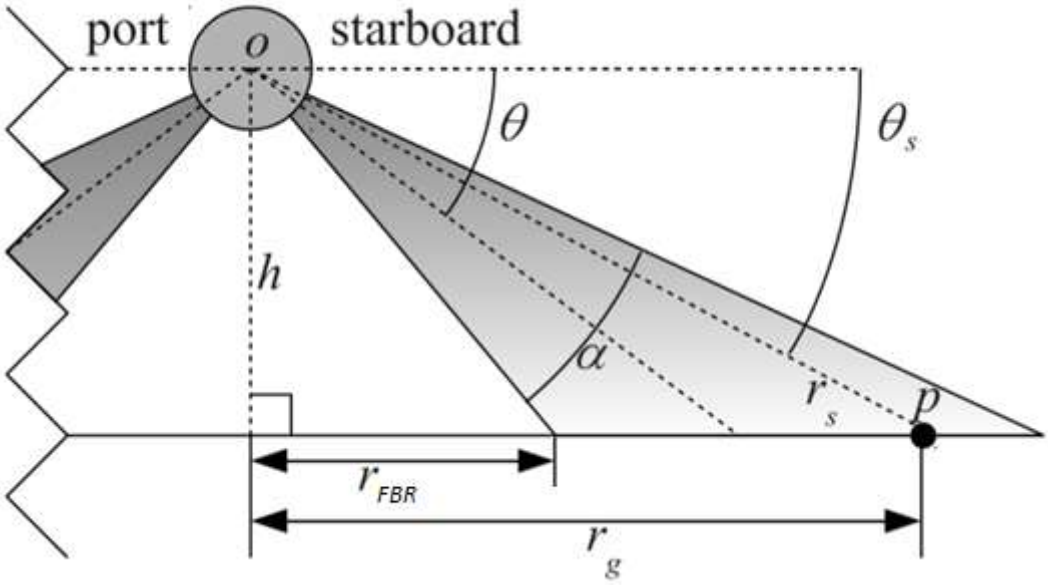

Figure 14 – AUV reference frame for nadir identification [64]

The initial returns of the side-scan sonar can therefore be determined from Equation (6).

$$r_{FBR} = \frac{h}{\cos\left(\theta + \frac{\propto}{2}\right)} \tag{6}$$

Where h is the AUV altitude corrected for roll and pitch, θ is 20 degrees and $\propto$ is 30 degrees.

Using the distance, $\boldsymbol{r_{FBR}}$, in metres, and the scale of metres/pixel orthogonal to the vehicles' travel across the TIFF image, the number of pixel values can be identified and removed from consideration in the inverse bathymetry calculations shown in Equation 4.

The nadir is not the only distortion in the side scan sonar images, there is also uneven insonification from the sonar. Values close to the nadir are over saturated and estimated to

be too high. This is seen in an example from an intensity profile return from [64] in Figure 15.

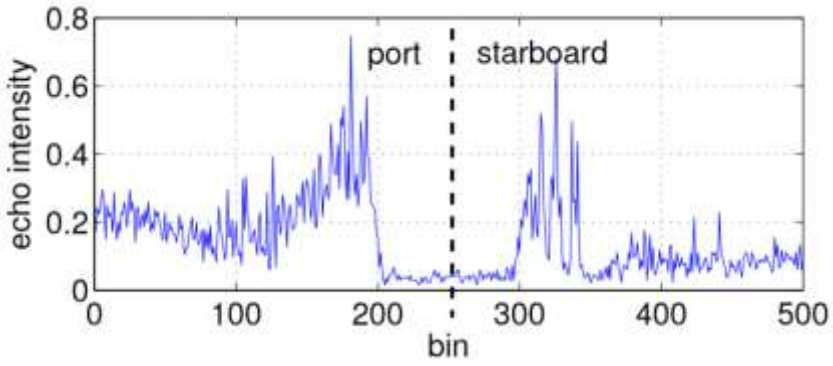

Figure 15 – Intensity values, showing the over brightened initial returns [64]

To obtain a more representative distribution of intensity values for the inverse bathymetry equation the images were scaled to intensity ranges from 0-1. It was important to understand the complexity of the sonar image to scale the image correctly. The IVER2 vehicles' SSS produce 8-bit images on a 0-255 scale, while IVER3 vehicles' SSS create 16-bit, 0-65536, unscaled images. The corrected scaling uses the unscaled TIFFs (16 bit) to produce (8 bit) scaled versions of the image. These accurately scaled images, from the IVER3 AUV, were then used in the elevation calculations, Figure 16a shows the original unscaled image and Figure 16b shows an 8-bit scaled version of the same image produced by the ATR.

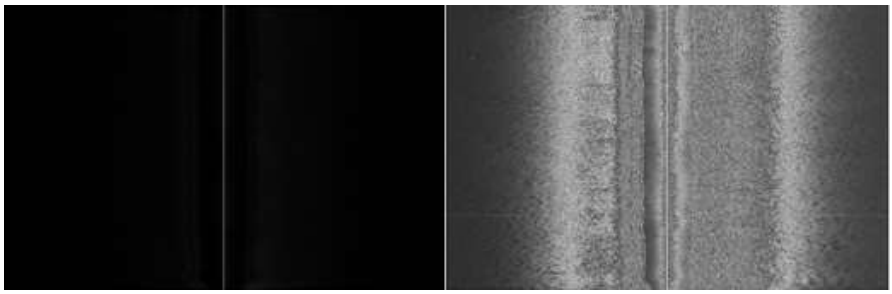

a. b.

Figure 16 – Unscaled port and starboard SSS images, unscaled (a) and scaled (b).

To correctly adjust the images, the nadir was not incorporated into the scaling, instead it was replaced in the final image for visual purposes with values of .5 on the 0-1 greyscale (exactly in the middle) as shown in Figure 17.

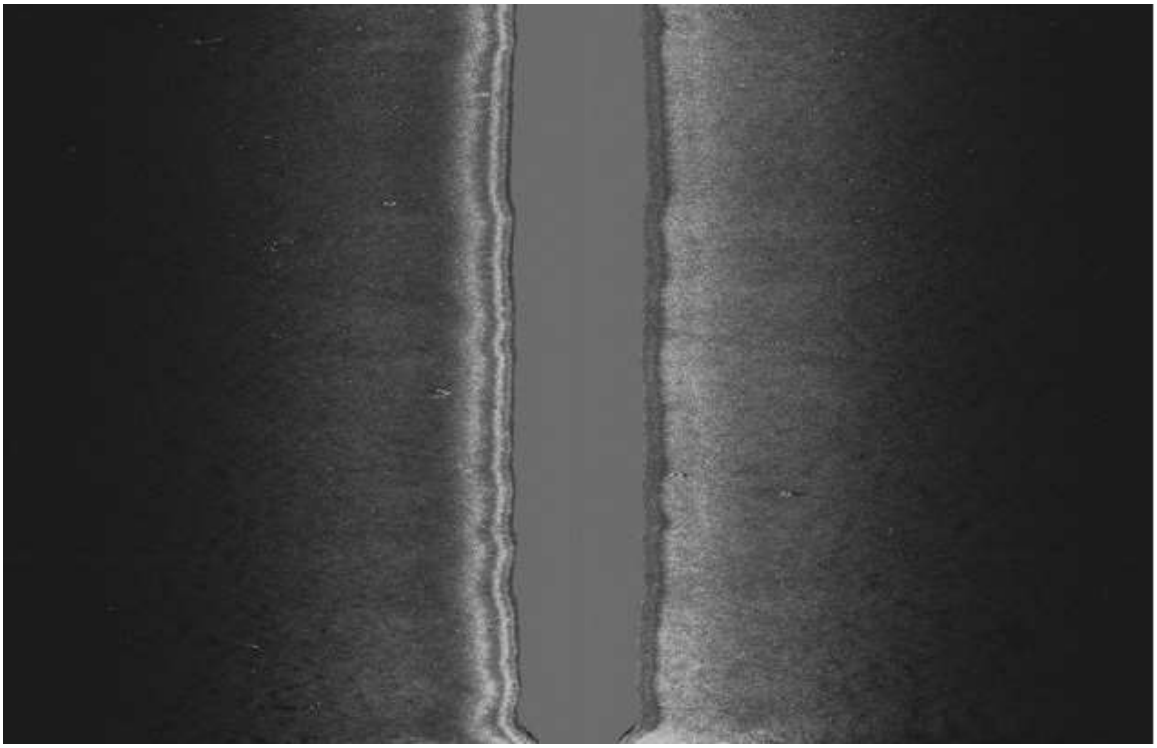

Figure 17 – SSS images for port and starboard mission leg, with intensity scaled and nadir removed

Not all scaling changes to the side-scan images were included in the initial calculations covered in section 4.2, where a convolution filter was used to smooth the image. This process was added after it became clear the generated bathymetry was affected by the scaling and nadir effects. The resulting bathymetries were far more consistent with what was expected, and allowed for improvements to the final association matches discussed in Chapter 5.

The altitude values, logged by the AUV, also had to be adjusted for the motion of the AUV as it traveled. The on-board INS sensed the vehicle's pitch and roll, and was used to adjust the AUV's altitude. While in many instances the pitch/roll values were minor (< 2 degrees) and not a factor in the sensor results there were instances of turbulent motion (>10 degrees) where this correction was critical to provide a sufficiently constant vehicle

position relative to each pixel value. This can be seen in the evaluation of the nadir from Figure 13 correctly identifying the first returned sonar value.

Another unexpected issue was the way the images were oriented coming out of the ATR. The port side images were rotated 180 degrees, while the starboard images were inverted along the orthogonal axis (perpendicular to the AUV's direction of travel). While this may be correctable by adjusting the ATR settings, accessing its source code was beyond the scope of this thesis. Instead the images were corrected after the ATR, but prior to the scaling and elevation extraction. Figures 18a and b show the before, while Figure 19a and b show the corrected versions of the port and starboard images for comparison.

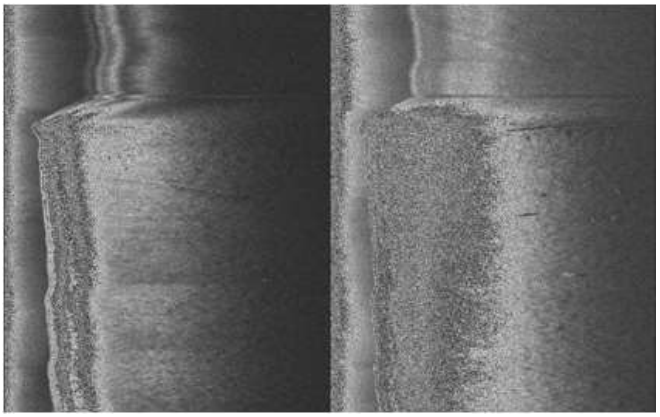

a. Port SSS image from ATR b. Starboard SSS image from ATR

Figure 18 – Unadjusted SSS images. Port (a) and starboard (b)

a. Port SSS image after adjustment b. Starboard SSS image after adjustment

Figure 19 – Adjusted SSS images, port (a) and starboard (b)

The corrected orientation of each image was individually validated by viewing the original raw side-scan sonar data using the MarineSonics SeaScanSurvey™ viewer. This issue appears to be caused by how Ubuntu creates the image files. In a Linux based OS the images are oriented as intended, while viewed in Windows OS for Matlab™ the images are rotated and inverted as shown in Figure 18.

4.1.4. Elevation Gradient Profiles

A set of feature data for each landmark can be created with the estimated bathymetry data from each generated TIFF image (referred to as the elevation map). The location of each target (landmark) within the TIFF image was calculated and stored as a single pixel. The row (y value) and column (x value) were found using data generated by the ATR. A data file was generated for each target and included the series of sonar pings it was observed in. The row of the TIFF image can be determined using the ping number (an ID tag for each ping value within a mission) of the target centre and the ping numbers at the beginning and end of the image the target was observed in. The distance to each target was also stored in the target data file as minimum and maximum distances in metres, as well as a scale across the image in metres/pixel. Finding the mid-point of these distances and converting to pixel distance yielded the column values.

The pixel value at the centre of the target allows the landmark's depth to be estimated within the elevation map. Depths at multiple other locations (also referred to, here, as zones) around the target were also sampled. A profile was made for each landmark for comparison against other landmarks by examining the change in elevation between the landmark and its surrounding zones. Figure 25 shows a basic conceptualization of this process.

With TIFF images, for this data set, ranging between 1300 × 1024 pixels and 3500 × 1024 pixels a singular pixel value provided a poor representation of the depth in each zone. Instead, a group of pixels, with the zone location as their centre, were used to determine an average altitude at each location. The TIFF image's scale (number of pixels per metre) was important to include when defining the number of pixels needed to average each zone's

depth as well as the number of pixels needed to ensure the zones were the correct distance from the landmark. The along-track (direction of vehicle travel) used a different scale [metres/pixel] than the across-track (distance out, normal to the vehicle travel direction). While the exact values change slightly for each leg of the mission depending on AUV speed, the along track scale was roughly 4 times as high as the across-track scale. Specific values for evaluation are further discussed in Chapter 5.

4.2. INITIAL TESTING AND RESULTS

Initial testing was performed using Matlab™, the scripts were then converted to C++ so that it could run on the IVER2 hardware-in-the-loop simulator installed on the back seat computer. This computer uses Ubuntu as its operating system. This testing performed a post-processing analysis on previously logged sonar data.

4.2.1. MATLAB TESTING

Side scan sonar data collected by DRDC based off the DRDC's Acoustic Calibration Barge in the Bedford Basin was evaluated in Matlab™ to determine if any data association trends could be gained. Figure 20 shows the AUV's path following a typical "lawnmower pattern". Each transect of the path (also referred to as a mission leg) creates both port and starboard side images.

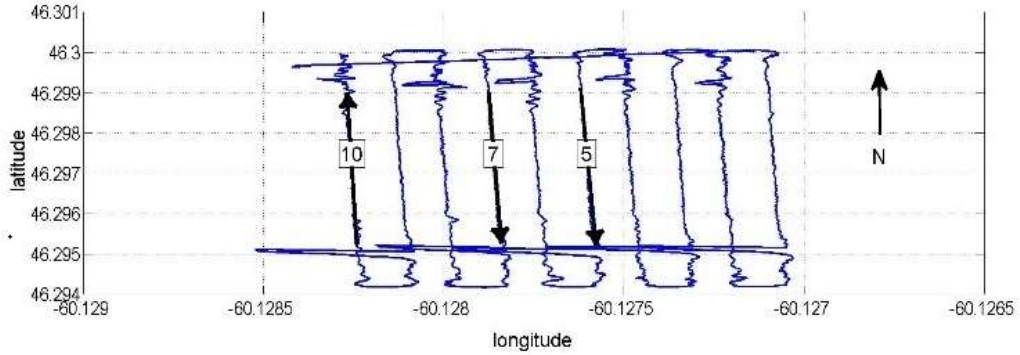

Figure 20 – AUV path for a NMCM survey with three mission legs highlighted

Three side-scan TIFF images were selected that contained landmarks within the sonar image intensity's optimal range to extract elevations. These images were taken from mission legs highlighted in Figure 20 (5, 7, and 10) and are shown in Figure 21. The

mission legs were approximately 450 metres in length and 12.5 metres apart. The landmarks from Figure 21 a (leg 10) and b (leg 7) were determined to be the same by comparing their latitude, longitude, and ranges from the AUV. Figure 21c was within an overlapping area but the landmark was found to differ from those in Figures 21a and b. In this figure, red boxes highlight correctly associated landmarks while a blue box shows an unassociated landmark.

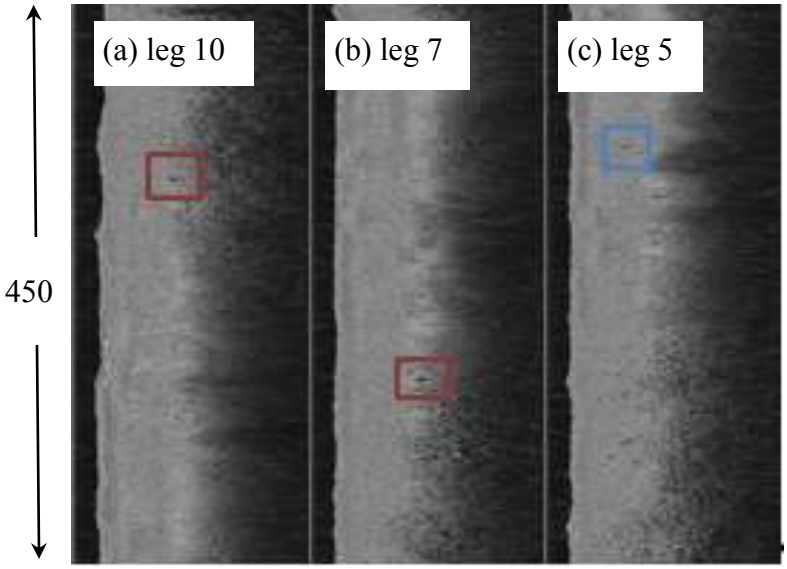

Figure 21 – Starboard SSS TIFF images matching the highlighted legs in Figure 20

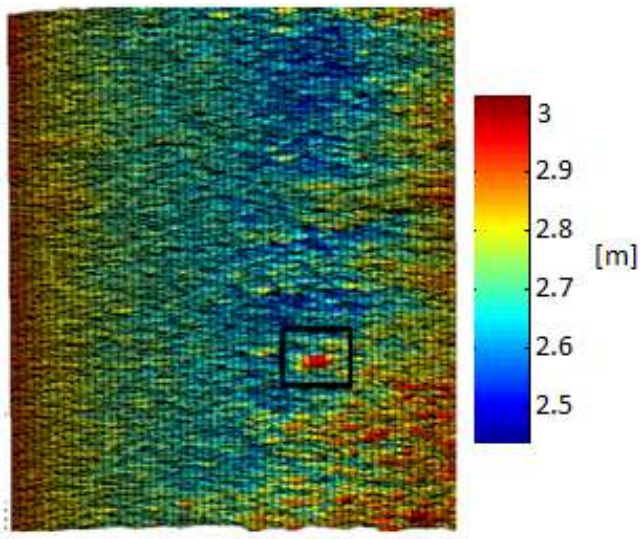

Figure 22 – Altitude approximation (Z map) of the seafloor for Figure 21 b, with the potential MLO highlighted

Elevation gradients centred around landmarks were calculated in the 4 cardinal (north, south, east, and west) directions. These 4 gradients, or slopes, were combined to form the landmark's elevation gradient profile. Evaluations were then done to compare profiles across landmarks. All landmark-to-zone distances and zone sizes were kept consistent across landmarks to ensure the results were directly comparable.

Several methods were tested to match elevation trends. The direction and magnitude of each gradient was independently examined, as well as the cumulative error – sum of the differences (errors) between each gradient.

Table 3 – Gradients between landmarks and N, E, S and W zones with error comparisons

	Zones			
Landmark est. Location	North	South	East	West
N-S leg 5	1.600e-04	1.052e-03	3.384e-04	5.686e-04
N-S leg 7	6.204e-04	1.160e-04	-4.002e-04	7.742e-04
Error leg 5 – leg 7	4.605e-04	9.357e-04	7.386e-04	2.057e-04
N-S leg 5	1.600e-04	1.052e-03	3.384e-04	5.686e-04
S-N leg 10	2.636e-04	5.071e-04	-2.411e-04	7.461e-04
Error leg 5 – leg 10	1.036e-04	5.446e-04	5.795e-04	1.775e-04
N-S leg 7	6.205e-04	1.160e-04	-4.002e-04	7.742e-04
S-N leg 10	2.636e-04	5.071e-04	-2.411e-04	7.461e-04
Error leg 7 – leg 10	3.569e-04	3.911e-04	1.591e-04	2.819e-05

At this point, the bathymetry that was calculated was of poor quality and a reflection of the lack of an on board INS as well as the bathymetry estimation algorithm implemented at that time. The highlighted data in Table 3 shows the calculated error between each slope

for landmarks in legs 7 and 10 (representing the correctly associated target). While not conclusively determining the targets in legs 7 and 10 represent a correct association and landmark 5 does not, there are two positive indications of a match. First the direction of the eastern slope for landmarks 5, 7 and 5, 10 is not consistent, while all directions for 7 and 10 are. Second the magnitude of the error for matching 7 and 10 was the lowest of all three for the eastern, southern and western slopes, while the northern slope error for 7 and 10 was less than that of 5 and 7. So only the northern slope of 5 and 10 suggested a better match than the known correct match. It is important to note that a certain portion of similar slopes are likely and can be expected when comparing targets within the same area even if the targets are not a correct match.

It was decided there were enough indications of positive association to continue examining this process as a viable method of improving the data association in underwater SLAM.

4.2.2. SIMULATOR TESTING

It is not only important that the process be theoretically sound, it must also be feasible within the processing limits of the AUV's on-board processor. Many factors (power, heat, cost) affect the backseat computer's on-board processing power, so prior to in-water trials the software was re-developed for testing on an AUV simulator. A hardware-in-the-loop simulator is, essentially, the processing core of the AUV. Since the test data was collected using the IVER2 AUV the simulator consisted of identical components to the AUV to ensure its ability to run in real-time.

In the simulator, near-raw sonar files and AUV state data (latitude, longitude, depth, speed, and heading) from previous missions were set up to load from the front seat to the back seat processors in, virtual, real–time. The back seat computer's performance in the simulator was directly comparable to its expected performance in a real mission. The simulations allowed us to determine if the code will be functional while other parallel mission processes are running, and if the software is robust enough to evaluate and return expected results within a timely mission interval.

A mission was reproduced on the simulator using another data set from the Bedford Basin experiments. The AUV path, shown in Figure 23 shows the first leg in red, with two subsequent legs highlighted in green and blue. The port and starboard SSS images from these legs, overlap roughly 75 % of the scanned area, as shown in Figure 24.

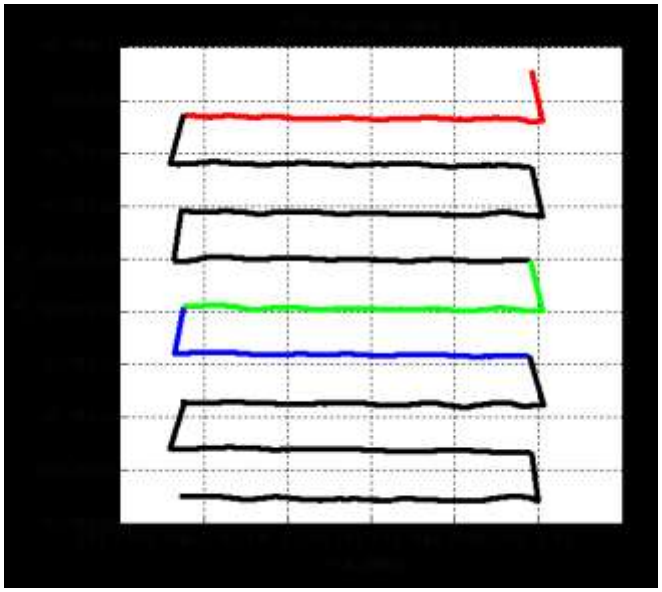

Figure 23 – AUV path for mission data used in simulator testing

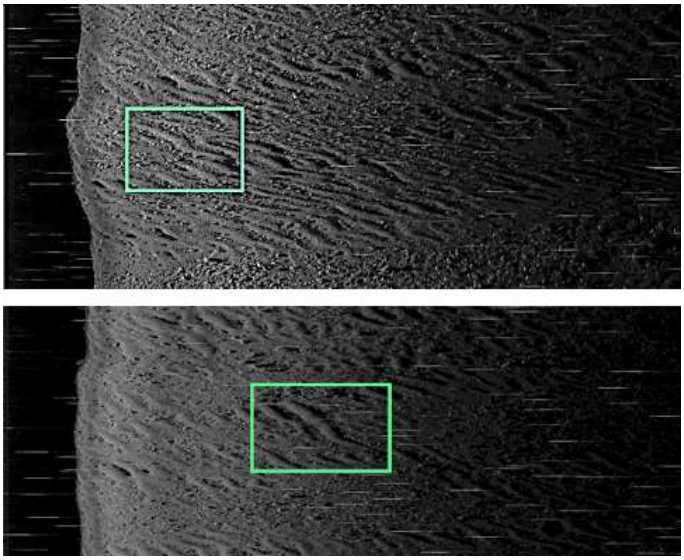

Figure 24 – Targets identified using ATR determined to be a match using seafloor elevations from the IVER2

While the identified targets in Figure 24 probably do not represent underwater mines, they were none-the-less matched to each other using the same process used for the initial Matlab™ testing. At this stage the elevation maps, target locations, and feature profiles were generated on the simulator and saved. The comparison of these profiles and the related image development (TIFF images, AUV path) were done using Matlab™ due to time restrictions and its simplicity of use. The final version of the algorithm will need to be coded in C++ for use by the AUV's back seat computer. The matching process, while not complete, functioned well within the limited time available during the mission. The exact time available for matching targets is directly related to the length and number of mission legs. The creation of bathymetry approximations uses the most processing time. This will cause a lag in time between target identification and development of a feature profile, but that is not expected to negatively impact its potential usefulness in SLAM.

CHAPTER 5. ALGORITHM VALIDATION

In order to optimize the functionality of the elevation extraction and application for matching specific seafloor locations a study was conducted on a data set using 5 separate parameters to determine a final association. Each parameter was adjusted individually to determine its unique impact on association outcomes. In this way we determined an idealized equation for evaluation. The parameters included:

- The number of zones surrounding the landmark,
- Whether or not the depth of the landmark was used (standard – Figure 25 or simplified – Figure 26),
- The number of pixels at each zone used to calculate an average depth for the area (resolution size),
- The distance from the landmark to each zone, and
- The threshold value below which an association is deemed correct.

The test set for this validation was acquired using the DRDC IVER3 in the Bedford Basin area with deployed targets. Two lawnmower patterns were performed orthogonal to each other and several months apart.

5.1. METHODOLOGY

Each landmark was identified by the ATR and given an identification label before any elevation testing. Landmarks, matched manually from the raw sonar data as observed in the SeaScanSurvey™ viewer, were used as a ground truth to determine the success of the elevation association.

The ideal algorithm was evaluated using the following criteria:

- Which test yields the most correct matches,
- Which test yields the fewest incorrect matches, and

- Which test operated in the least amount of time (reducing the loading on the embedded processor).

Trials were split into two primary categories, across-track (four zones, in front, behind, to the port and to the starboard of the landmark, Figure 25) and along-track (two zones, only in front of and behind the landmark, Figure 26). Trials were further split into two more categories, standard and simplified. The standard version looked at the elevation changes between the landmark and corresponding zones, while the simplified method removed landmark depth from consideration to simplify the computational time as well as removing potential error in situations where landmarks cast a large shadow. In each case elevation changes between zones were compared (for example, from the port zone to the starboard zone).

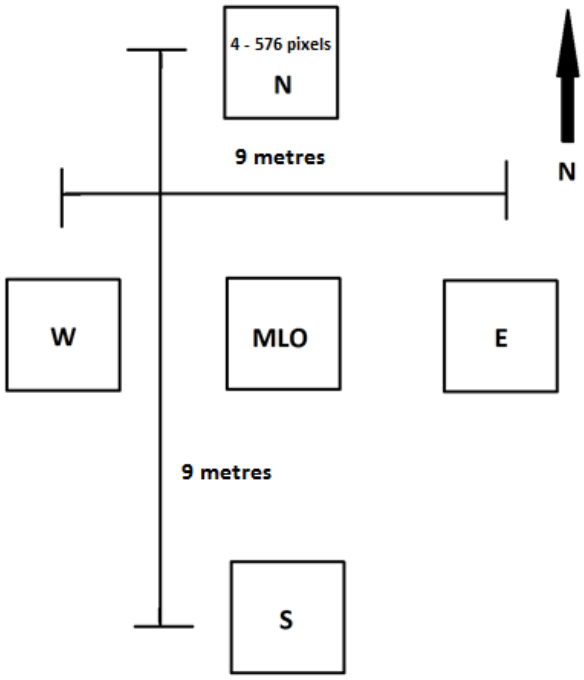

Figure 25 – Across-track method layout, assuming a north-bound AUV heading

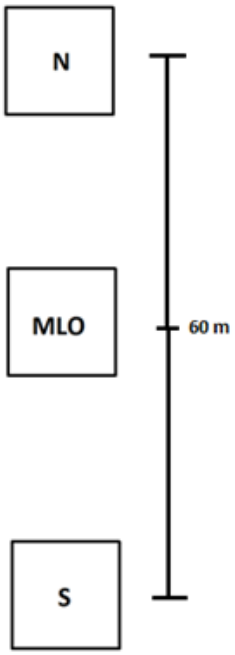

Figure 26 – Along-track method layout, assuming a north-bound AUV heading

The series of gradients (slopes) stored for each landmark make up its elevation profile. Two landmarks were compared for an association using a root mean square method as shown in Equation (7):

$$\sqrt{\frac{\sum_{n=1}^{n=\#\ of\ zones} Z_n^2}{n}} < threshold\ value. \tag{7}$$

Where, Z_n is the difference between the gradient from the landmark to zone *n* (for the first landmark being associated) and the gradient from the landmark to zone *n* (for the second landmark being associated). Where *n* can be the integer values of 1, 2, 3 or 4 corresponding to the zones in front of, behind, to the starboard or port sides of the landmark, respectively.

$$Z_n = Gradient_{to\ zone\ n}^{landmark\ 1} - Gradient_{to\ zone\ n}^{landmark\ 2} \tag{8}$$

An example of an across-track, standard equation would appear as shown in Equation (9):

$$\sqrt{\frac{(Z_1^2 + Z_2^2 + Z_3^2 + Z_4^2)}{4}} < Threshold \tag{9}$$

As mentioned above, many tests used only data from zones 1 and 2. The threshold value was determined through a series of tests with ranges between 0.03 – 0.005 yielding the best, most consistent results depending on the data set being used. These threshold values were determined using trial and error adjustments until positive trends were established. Thresholds set too high allowed for too many association matches, while too low allowed for none.

The distance from the landmark to the evaluation zones was varied from 5 to 25 metres and the number of pixels used to average the depth (resolution) at each zone was varied between 4 and 576. These values were set by the minimum and maximum allowable sizes based on the size of the SSS images. The distance and resolution values were changed independently and associations were evaluated for each combination. 24 landmarks, within mission 1, allowed for 1,190 different associations that were theoretically possible.

After searching for a singular distance and resolution value it was determined that a more reliable method would be to record all associations for a range of distances and resolutions and search for the matched sets which appeared most often. The more often a match was achieved the more likely it was considered to be correct. The initial results contained a large number of associated pairs that were incorrectly matched. This indicated that in some situations the elevation profiles could not act as the data association on their own. In these instances landmarks that were beyond a nearest neighbour threshold (a distance based on the dead-reckoned position of the AUV when each landmark was observed) were not considered. The distance threshold was based on the reach of the SSS itself (~40 metres) and the distance between each mission leg (also ~ 40 metres). Targets that were farther then 80 metres (2 mission legs) would not be able to associate. This is made possible due to the high quality INS on the IVER3 AUVs used so that the dead-reckoned position of the AUV is fairly accurate even through a mission of several hours in duration.

5.2. TESTING

The IVER3 UUV mission used for algorithm validation was conducted in the Bedford Basin area with deployed targets on two separate occasions using lawn mower patterns orthogonal to each other. Mission 1 (Figure 27) was a North West – South East run with the DRDC ATR identifying 20 potential mine like objects. Mission 2 (Figure 27), was conducted 2 months later (when landmarks may have shifted or become partly covered with sediment) with only 8 potential MLOs identified.

Searching two data sets for both position based and gradient associations yielded landmark matches with significantly increased reliability. The data set covered an area of approximately 50, 000 m^2, in a relatively flat harbour. The ATR detected 24 landmarks (MLO) within mission 1 and 8 within mission 2. This low number of landmarks returns in each mission is due to the relatively sparse operating area and the high quality of the sonar (900 kHz).

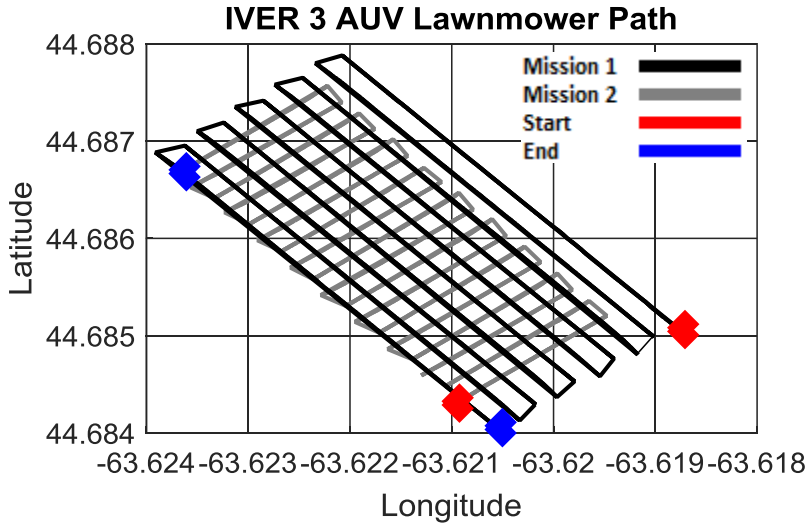

Figure 27 – AUV lawnmower path for two missions with the starting points in red and ending points in blue

The results for Cases 1 – 5, discussed in Chapters 5.2.1. – 5.2.5, all use data from only mission 1. This is because to find an association the ATR must identify the same target within two separate SSS images. This only happens within the mission 2 data set once. Mission 1, on the other hand, has 7 landmarks identified by the ATR and that appear in multiple images. These landmarks were independently confirmed by manual inspection of

the near-raw sonar data. This makes mission 1 data a much larger sample size to draw conclusions from.

Figure 28a shows a SSS TIFF after smoothing with the nadir filled in as a grey bar. Figure 28b shows a 3 dimensional representation of the same image as determined by Equation (1). The blue boxes show an example of an easily observed feature within both images. The red boxes show the location of a series of rocks that the ATR classified as a potential MLO (landmark) in both images.

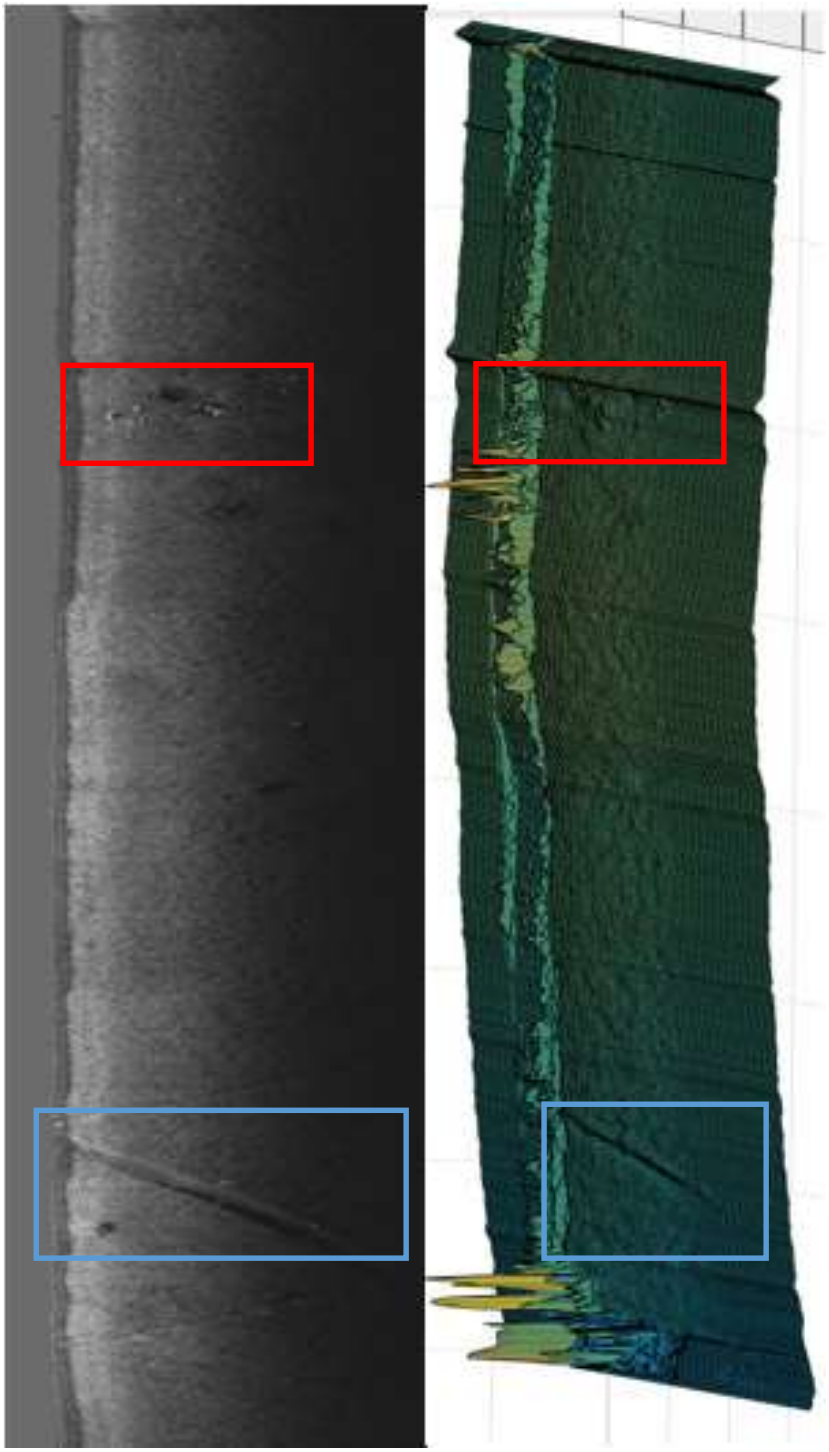

a. **b.**

Figure 28 – An example of a side-scan sonar image 3501×1024 pixels (a) and alongside its estimated bathymetry map (b)

A close up of these rocks (the red box) from the sonar image is shown in Figure 29. Within this SSS image the ATR identified 2 separate potential MLOs, while in the next view of the same cluster of rocks only 1 MLO was identified.

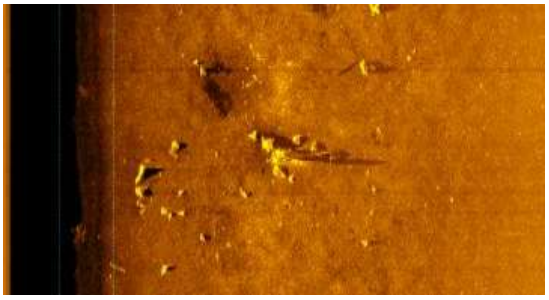

Figure 29 – ATR landmarks, WP 33 – starboard

Figure 30 shows the same cluster of rocks (only 1 ATR MLO) viewed from the next leg of the mission.

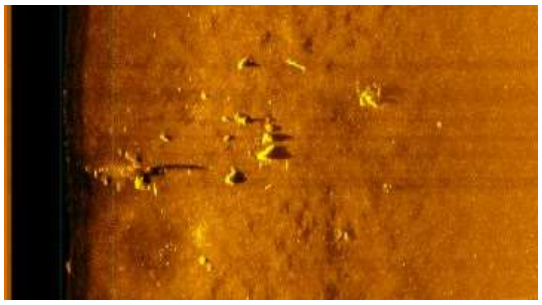

Figure 30 – ATR landmark, WP 37 – starboard

Mission leg numbering as shown in Table 3 increased in increments of 4, starting with a value of Waypoint #5 for the first leg of each mission.

Table 4 – Labelling the actual leg number of a mission compared to the values labelled on the raw sonar data files

Actual Leg Number	Mission 1 WP Numbers	Mission 2 WP Numbers
1	5	5
2	9	9
3	13	13
4	17	17
5	21	21
6	25	25
7	29	29
8	33	33
9	37	37
10	41	41
11	-	45
12	-	49
13	-	53
14	-	57
15	-	61
16	-	65
17	-	69
18	-	73

Matched landmarks were labelled by the mission waypoint number (leg number) and target ID number. For example a combination of starboard WP17, target #2 and starboard WP21, target #1 was labelled s172s211.

5.2.1. CASE 1: ALONG-TRACK, SIMPLIFIED METHOD

The along-track method allows for evaluation of more landmarks and at larger distances around the landmark. Some landmarks can appear differently from one SSS image to the next even if they are the same target (typical of SSS imagery). A common change in appearance is a fluctuation in the brightness of the target (indicating its height) and the size of its shadow. The resolution of pixels used to average landmark depth is highly affected by its position within the TIFF as identified by the ATR. Even a small shift in these values can result in incorporating too much of the landmark's shadow in the evaluation, altering its perceived depth. It was purposed that not including the landmark depth could remove this issues.

The correctly associated landmark pairs were manually verified and are highlighted by the green bars as shown in Figure 31. This left a number of blue bars that were incorrectly associated multiple times. Figure 31 shows these results for the along track, simplified data for mission 1 without considering landmark depth while Figure 32 includes landmark depth.

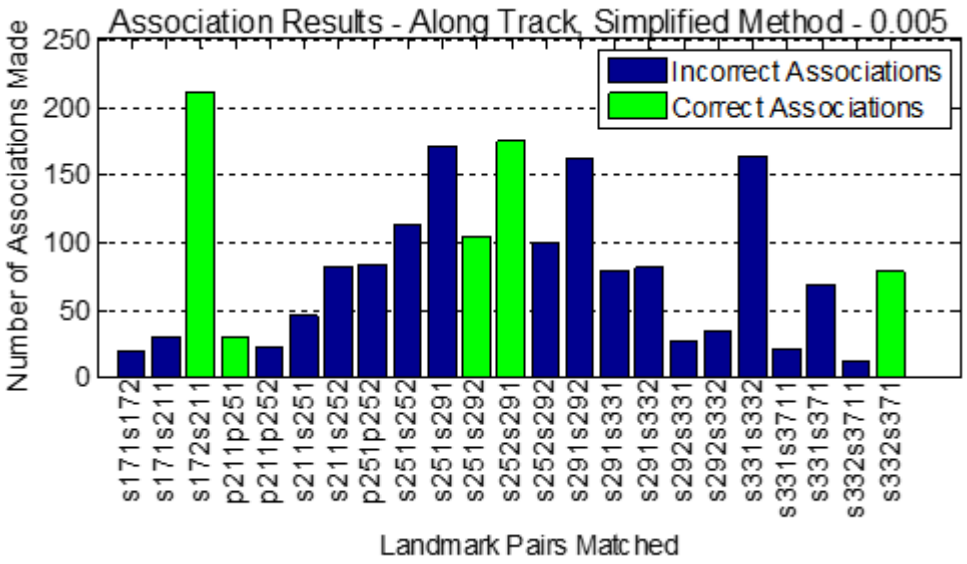

Figure 31 - Pairs of landmarks matched using the along–track elevation profile component, simplified approach and an association threshold of 0.005

5.2.2. CASE 2: ALONG-TRACK, STANDARD METHOD

The standard method, as previous outlined, was the initial testing process for creating elevation profiles. This method, including the extended range available with the along track method (Figure 26), resulted in the mission 1 results set is shown in Figure 32.

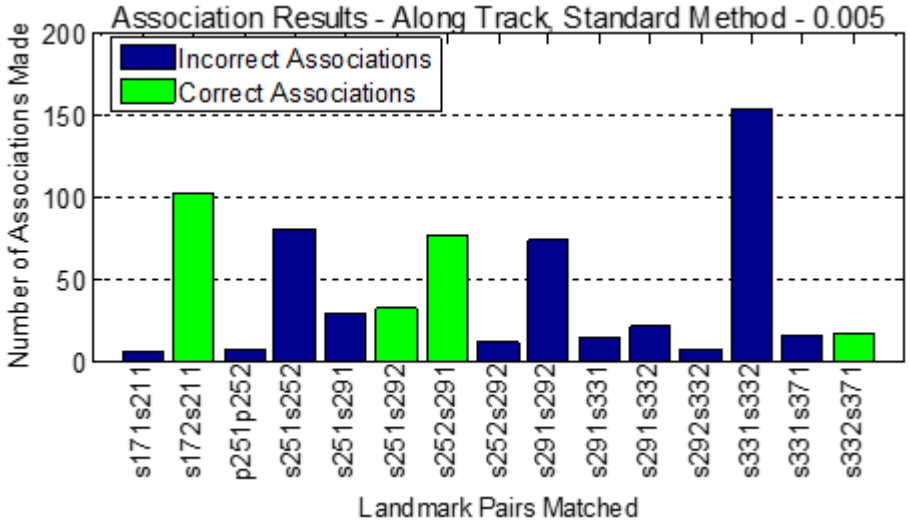

Figure 32 – Pairs of landmarks matched using the along track, standard approach and an association threshold of 0.005. Incorrect associations (blue) have been greatly reduced compared to Case 1

There are fewer pairs that match at the same threshold value used in Case 1. However many more of the correctly associated pairs persisted and the remaining blue bars have been substantially reduced. Of the largest three remaining blue bars all can be discarded because they represent matching landmarks from a single SSS image (associations require at least 2 views of a landmark from separate SSS images). They appear in the results only because all possible combinations of the 24 landmarks were allowed to attempt a match. Some of these instances (such as s331s332) offer close matches because of their small relative distance to each other while others (e.g. p251p252) also from a single image are farther apart and associated less frequently. As a set the along-track results using the standard method of evaluation were a clear improvement over the simplified method.

5.2.3. CASE 3: ACROSS-TRACK, SIMPLIFIED METHOD

The primary reason for using the across-track method for analysis is that it opens up the possibility of matching landmarks that were viewed from orthogonal runs. The primary disadvantage, as previously stated, is the maximum distance for an evaluation zone is a function of the swath length of the SSS. If the zones in the direction of AUV travel (along-track) are of different lengths, the zones in the across-track can no longer be used for orthogonal matching.

As part of the evaluation we first tested the across-track method using only the data from mission 1 instead of combining both mission data sets. This was done to compare the values from the across-track method to the results from the along-track method.

The MarineSonics SSS on the IVER3 swath is approximately 40 metres, however after removing the nadir only targets well centred within the SSS image can be used and at a maximum distance of 9 metres. Therefore, the simplified version of the across-track method reaches distances up to 18 metres. The Across-Track, Simplified Method results using a 0.005 threshold are shown in Figure 33.

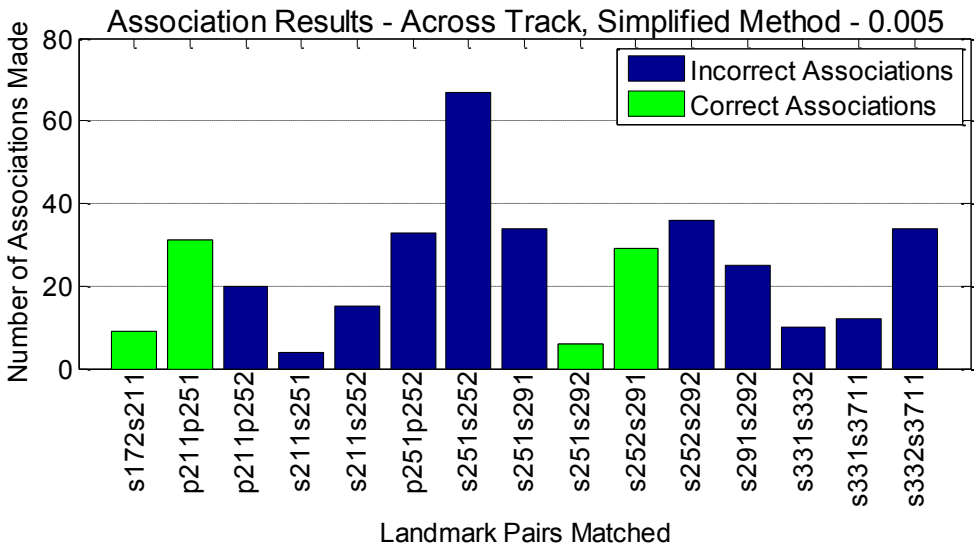

Figure 33 – Pairs of landmarks matched using the across-track, simplified approach and an association threshold of 0.005. Improved number of correct associations, with many incorrect associations coming from a single SSS image

These results were found to be fairly good. While not as many correct associations are observed 4 were still found and p211p251, which was almost completely missed by the along track method, has a strong association here. In addition many of the blue columns were found to be landmark pairs from a single image. Also of note, the incorrect matching of the pair of landmarks from WP 25 and 29 have become more frequent then the correct combination, which is consistent with the results at this stage for not including target depth.

5.2.4. CASE 4: ACROSS-TRACK, STANDARD METHOD

After including the target depth it was found that the 0.005 threshold was too high to allow for associations. The threshold value was increased to 0.015 and 0.01 and the results are shown in Figures 34 and 35 respectively.

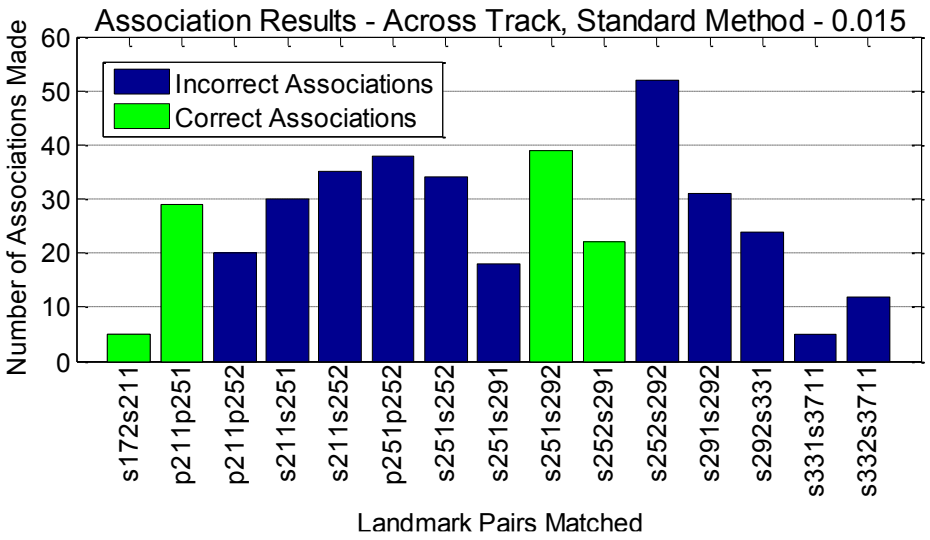

Figure 34 – Pairs of landmarks matched using the across track, standard approach and an association threshold of 0.015. Some correct matches, but many incorrect matches as well

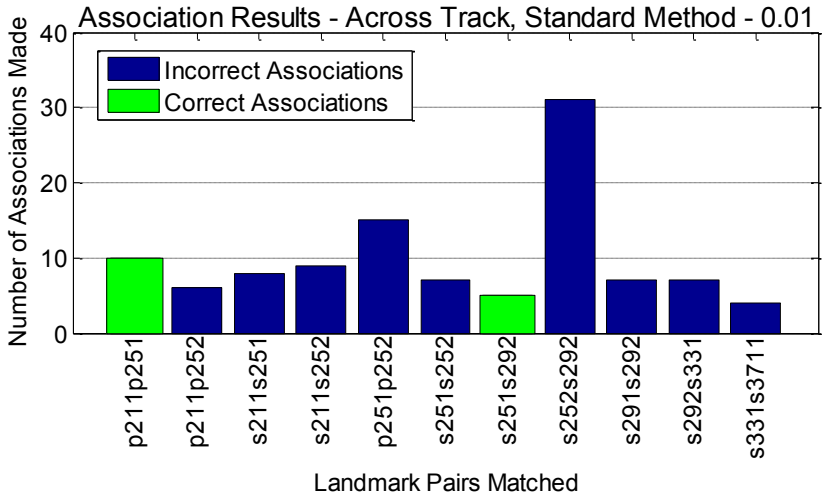

Figure 35 – Pairs of landmarks matched using the across track, standard approach and an association threshold of 0.01. Threshold is too low for correct matches, but still has incorrect ones

The change in threshold between 0.015 and 0.01 has a significant effect on association results. Both sets show some positive information with many of the incorrect associations being the same expected values as before. The threshold of 0.01 was found to be too high, and removed too many of the correct associations. The concern with this method, is that inclusion of landmark depth increases the number of incorrect as well as

the correct associations for landmarks grouped together. The simplified version of the across-track method yielded the best results using this data set.

5.2.5. CASE 5: ASSOCIATIONS FROM ORTHOGONAL HEADINGS

After combining across-track values from missions 1 and 2 the best results were determined to be a product of the standard method. Combining the two data sets created an overlap in the naming convention of several MLO and association pairs listed in the bar graph results. To separate these landmarks MLOs from mission 2 were appended with "90" to keep in line with the original SSS data naming convention, as mission 2 was rotated 90 degrees in heading from mission 1. For example the green column in Figure 36 labelled s211s29290 shows the correct association from mission 1 starboard – WP21, target #1 and mission 2 starboard – WP29, target #2. These results at thresholds of 0.03 and 0.06 are shown in Figures 36 and 37 respectively.

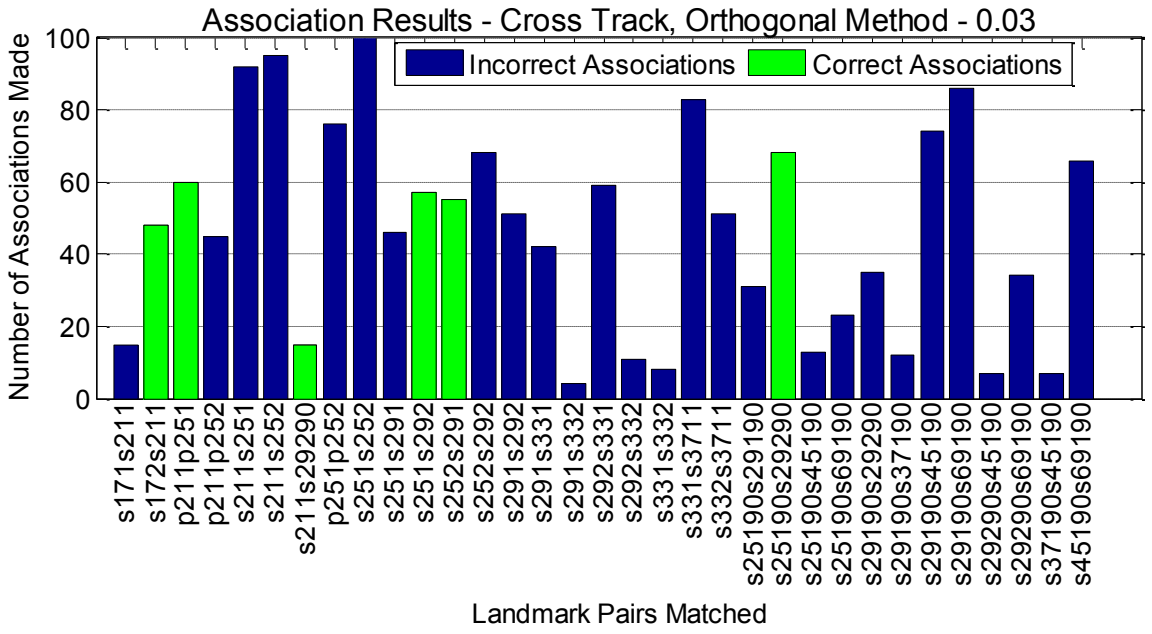

Figure 36 – Orthogonal pairs of Landmarks matched using the across track, standard approach and an association threshold of 0.03. Incorrect associations appeared in higher numbers than correct ones

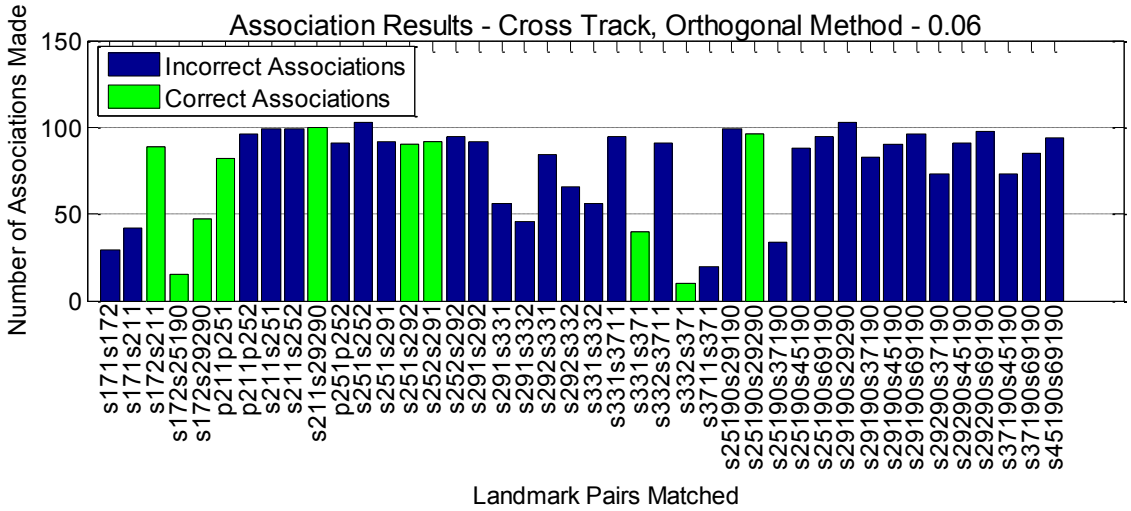

Figure 37 – Orthogonal pairs of Landmarks matched using the across track, standard approach and an association threshold of 0.06. The increased threshold did not produce more correct associations

The orthogonal matches have not been a success to date. While correct orthogonal associations were more consistently measured when the threshold was raised to 0.06, so were the associations of most possible matches. Figure 37 shows an association cut-off so high that almost all possible matches were found.

These figures also show mission 2 landmarks being matched to each other. With threshold values this high the associations using mission 2 data were not valid or useful. The mission 2 data when evaluated on its own with a 0.005 threshold yielded the results in Figure 38. With only 8 ATR landmarks within a large area this data set was sparse enough that no estimated position was required to achieve successful associations. Most possible landmark combinations had 0 associations and the one correct pair (s251s292) matched more frequently than any other.

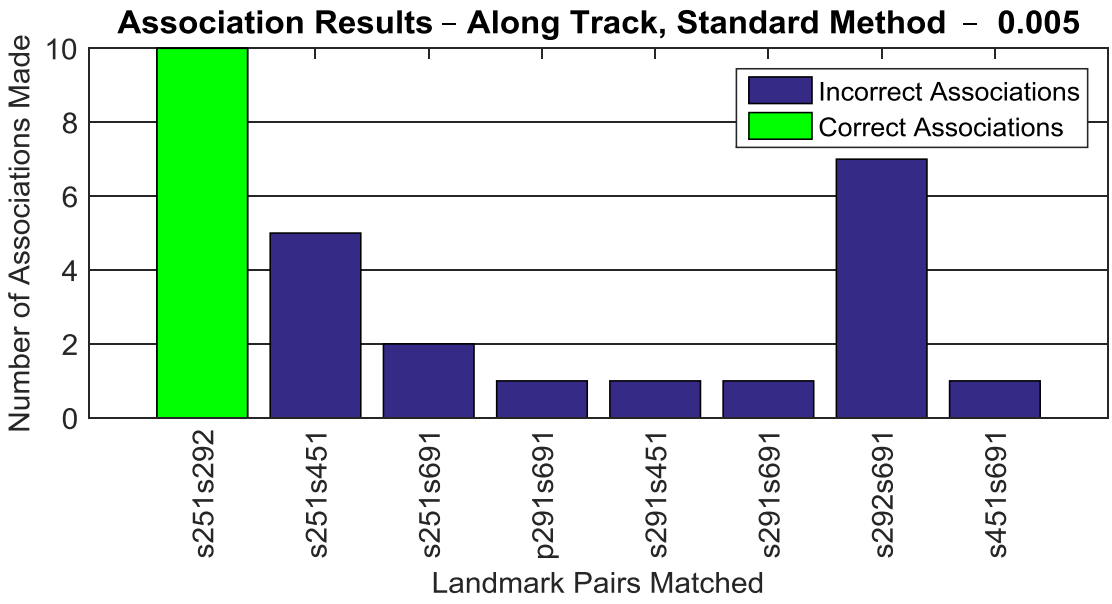

Figure 38 – Pairs of landmarks matched using the along track, standard approach and an association threshold of 0.005 for mission 2 data. This dataset also has its best results when using the method in Case 2

5.3. DISCUSSION

Each of the 5 testing methods outlined to this point have associated landmark pairs, showing matches we know to be incorrect, in blue. Some of these are expected and are explained in this section.

When the landmarks are positioned close together on the seafloor they will often have similar elevation profiles. This can cause matches when two landmarks are viewed within only one image. A good example of this s331s332 in Figure 32, and the rocks shown in Figure 29. Furthermore, two landmarks from the same image can be expected to match closely based on local gradients, but logically can be removed from further consideration.

Within the starboard images of leg 25 and 29 (concurrent legs) two landmarks each were identified and correctly associated as s251s292 and s252s291. Figure 32 shows the reverse of these associations (s251s291 and s252s292), which were also matched in several cases. As mentioned whenever landmarks are closely grouped on the seafloor as shown in Figures 29 and 30, this is to be expected. It is important to note that association matches

including landmark depth produced much better results (Figure 32) compared to those where depth was excluded (Figure 31).

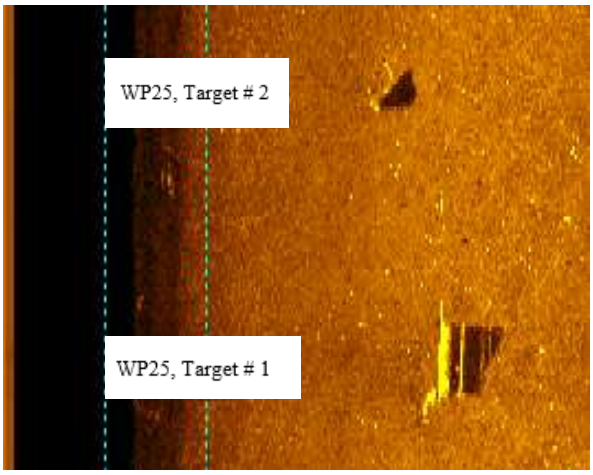

Figure 39 – ATR landmarks 1 and 2, WP 25 – starboard

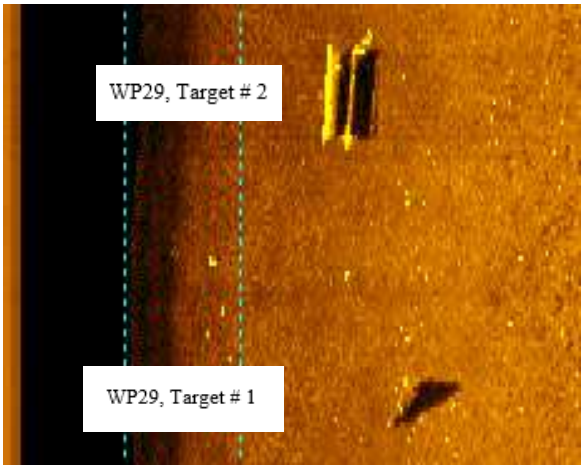

Figure 40 – ATR landmarks 1 and 2, WP 29 – starboard

The most consistent correct association pair for both data sets was WP 17 – starboard, target #2 and WP 21 – starboard target #1. These targets are shown from both views in Figures 41 and 42. It is believed the success of these matches was a result of the sparsity of the immediate environment and their clear representation within the TIFF.

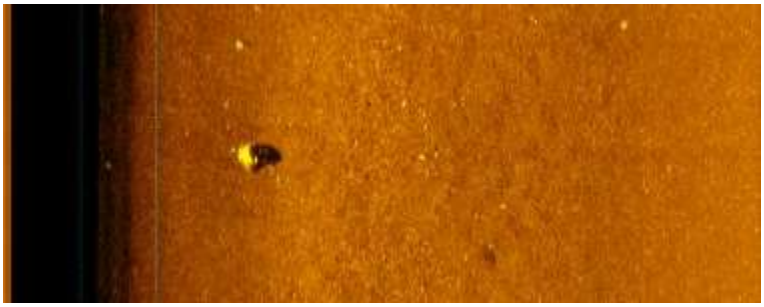

Figure 41 – ATR landmark, WP 17 – starboard

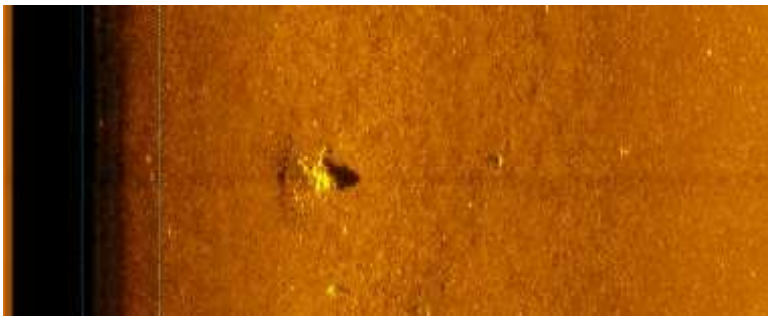

Figure 42 – ATR landmark, WP 21 – starboard

Errors discussed so far have focused on failing to avoid incorrect associations while none of the evaluation methods were able to make all correct associations. In Chapter 5.2.1. it was suggested this might be caused by landmarks with larger shadows (and consequently more oblique aspects). For example WP41 – port, target #1 and WP37 – port, target #1 are ATR results for a car on the seafloor, which are shown in Figure 43 and 44 respectively.

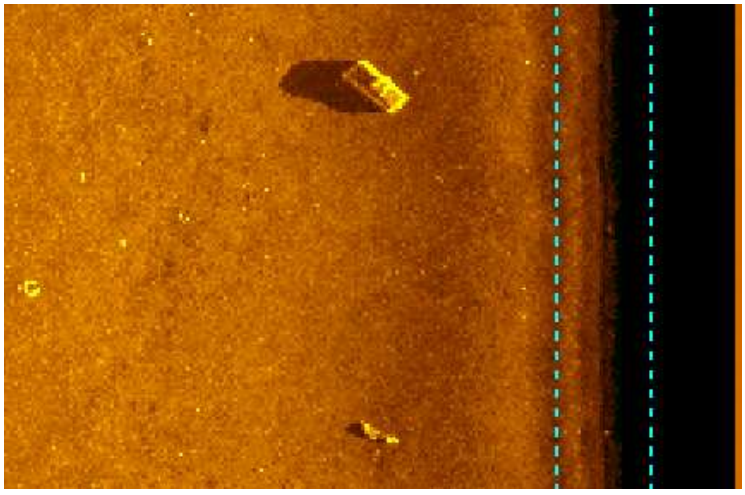

Figure 43 – ATR landmark (car), WP41 – port

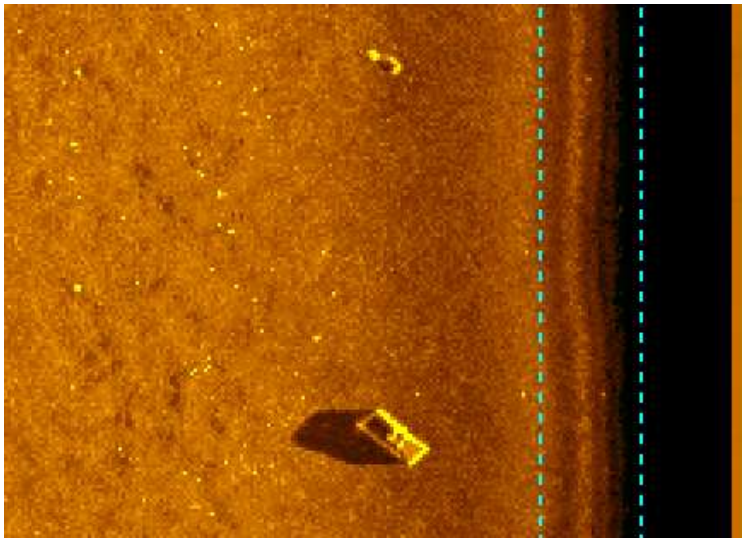

Figure 44 – ATR landmark (car), WP37 – port

Of the all of the testing combinations examined in this thesis the most useful results came from the Along-Track – Standard Method. Figure 45 shows the same bar graph from Figure 32 with the matched pairs from a single mission leg colored orange since they can be safely disregarded. The figure shows 5 out of 7 landmarks were correctly associated. While some blue columns remain they are on average smaller than the correct associations and can be accounted for due to the circumstances such as proximity to other landmarks.

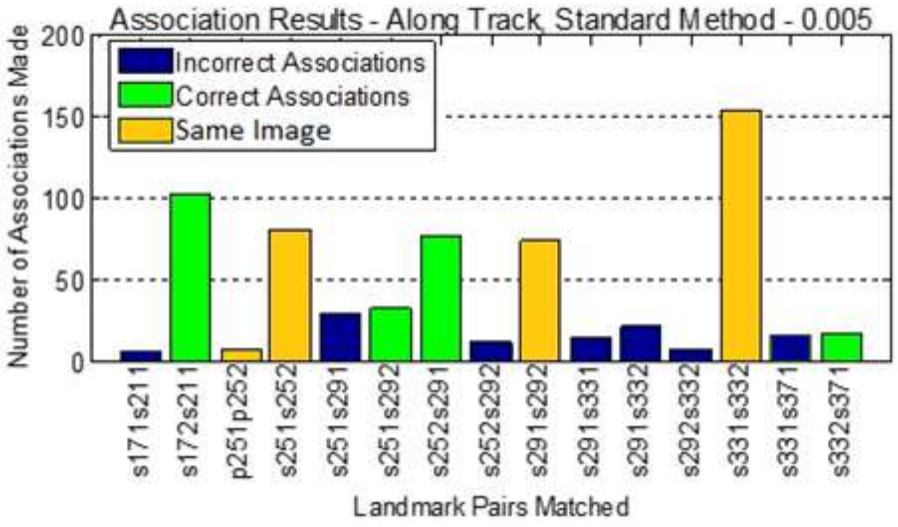

Figure 45 – Pairs of landmarks matched using the along track, standard approach and an association threshold of 0.005 and removing associations from the single images

CHAPTER 6. DIRECTION OF FUTURE RESEARCH AND CONCLUSIONS

This thesis has developed and tested a novel method to augment data association with the aim to strengthen the association. While a landmark's orientation may change or be in various stages of burial/uncovering from the seabed over days or months, it is unlikely the surrounding seabed gradient will change as quickly. Combining distinctive and enduring features like the local seabed gradient, jointly associated with the NN estimated position, was found to facilitate the SLAM process leading to more consistent and accurate results. In this way, the persistence (over longer time interval) is seriously addressed in the data association. As well, if a new landmark is introduced to the environment the local seabed gradient association will reinforce and highlight the change.

The data association scheme proposed is computationally efficient, it adds little processing to what is already being implemented on an embedded processor using JCBB. Additionally, it exploits unused parts of the same SSS image that landmarks are extracted from, with no additional runs or sensors required.

There are a number of avenues of future research that could be examined to further develop the thesis' theories and accomplishments.

1. MLOs can be large enough to cast a substantial shadow, reducing the effectiveness of the association process. Using the simplified method reduces this problem but has its own short comings separating landmarks within a cluster. To address this moving forward the landmark's resolution could be set independently of the remaining evaluation zones. This is expected to reduce noise caused by the shadow around the landmark while maintaining the improved depth estimation associated with a higher resolution for the non-landmark zones.

2. The accuracy of associations using seafloor gradients is a function of the quality of available SSS data. More detailed bathymetry would improve the accuracy of elevation profiles, and overall association outcomes. The DRDC IVER3 AUVs are already equipped with high quality SSS, DVL and INS so the input data is reliable. To improve the estimated bathymetry, future

research should focus on accurate TIFF scaling to more consistently reduce the uneven insonification. Another method to improve the bathymetry would be to use an interferometric SSS. These sonars can create bathymetry profiles on their own and this would remove the most computationally intensive aspect of elevation profiling for data association. DRDC is in the process of securing an IVER3 UUV with interferometric bathymetric sonar and a SSS.

3. Improving the orthogonal matching functionality will be critical for successful use of this algorithm in real world applications. Mission surveys will not always be able to maintain the constant headings required for Along-Track associations. Surveys incorporating multiple AUVs traveling at different headings will also not be possible without this development. For this to progress SSS with wider swaths, greater than the current 40 metres, must be used to increase the number of sampling points around a landmark. This can be achieved using the current sonars by fusing two estimated bathymetry maps from the port and starboard sides of a single mission leg. This would double the width of the map with only the nadir unusable for creating elevation profiles.

As of September 2015 the most up to date version of the elevation gradient data association algorithm is installed on the backseat payload computer of DRDC's IVER3 AUV. As sonar files are generated the ATR software locates potential MLOs before passing this information to the elevation profile software. Initial in-water trials are complete and the analysis is ongoing. The work from this thesis proves the hypothesis that there is a great deal of merit in using the seabed elevation profiles to augment the data association for underwater SLAM.

REFERENCES

[1] F. Dellaert and M. Kaess, "Square Root SAM: Simultaneous Localization and Mapping via Square Root Information Smoothing," *The International Journal of Robotics Research,* vol. 25, pp. 1181-1203, 2006.

[2] H. Durrant-Whyte and T. Bailey. Simultaneous localization and mapping: Part I. *Robotics & Automation Magazine, IEEE 13(2),* pp. 99-110. 2006.

[3] M. L. Seto and H. Li. On-board AUV autonomy through adaptive fins control. Presented at 2010 IEEE Conference on Automation Science and Engineering (CASE), 2010.

[4] (March, 2013). *Affordable Next Generation Autonomous Underwater Vehicle (AUV)*. Available: http://www.iver-auv.com/Iver2_AUV_Brochure.pdf.

[5] M. L. Seto. *Marine Robot Autonomy* 2012.

[6] K. Nagothu, M. Joordens and M. Jamshidi. Communications for underwater robotics research platforms. Presented at 2008 2nd Annual IEEE Systems Conference, 2008.

[7] D. Anguita, D. Brizzolara, G. Parodi and Qilong Hu. Optical wireless underwater communication for AUV: Preliminary simulation and experimental results. Presented at IEEE OCEANS, 2011.

[8] J. Borden and J. DeArruda. Long range acoustic underwater communication with a compact AUV. Presented at IEEE OCEANS, 2012.

[9] H. P. Yoong, K. B. Yeo, K. T. K. Teo and W. L. Wong. Modeling of acoustic channel for underwater wireless communication system in AUV application. Presented at 14th International Conference on Computer Modelling and Simulation (UKSim), 2012.

[10] Zhu Wei-Qing, Wang Chang-hong, P. Feng, Zhu Min, Wang Rui, Zhang Xiang-Jun and Dai Yong-Mei. Underwater acoustic communication system of AUV. Presented at OCEANS, 1998.

[11] G. A. Hollinger, S. Choudhary, P. Qarabaqi, C. Murphy, U. Mitra, G. Sukhatme, M. Stojanovic, H. Singh and F. Hover. Communication protocols for underwater data collection using a robotic sensor network. Presented at 2011 IEEE GLOBECOM Workshops (GC Wkshps), 2011.

[12] T. P. Trappenberg, "Learning with Robots," *Dalhousie University,* 2013.

[13] J. C. Kinsey, R. M. Eustice and L. L. Whitcomb. A survey of underwater vehicle navigation: Recent advances and new challenges. 2006.

[14] R. Martinez-Cantin and J. A. Castellanos. Bounding uncertainty in EKF-SLAM: The robocentric local approach. Presented at Proceedings 2006 IEEE International Conference on Robotics and Automation, 2006.

[15] A. Burguera, G. Oliver and Y. González. Range extraction from underwater imaging sonar data. Presented at 2010 IEEE Conference on Emerging Technologies and Factory Automation (ETFA), 2010.

[16] J. Mullane, Ba-Ngu Vo, M. D. Adams and Ba-Tuong Vo. A random-finite-set approach to bayesian SLAM. *Robotics, IEEE Transactions On 27(2),* pp. 268-282. 2011.

[17] S. Thrun, W. Burgard and D. Fox. *Probabilistic Robotics (Intelligent Robotics and Autonomous Agents)* 2005.

[18] J. Li, L. Cheng, H. Wu, L. Xiong and D. Wang. An overview of the simultaneous localization and mapping on mobile robot. Presented at 2012 Proceedings of International Conference on Modelling, Identification & Control (ICMIC), 2012.

[19] Jeong-Gwan Kang, Won-Seok Choi, Su-Yong An and Se-young Oh. Augmented EKF based SLAM method for improving the accuracy of the feature map. Presented at 2010 IEEE/RSJ International Conference on Intelligent Robots and Systems (IROS), 2010.

[20] T. Bailey and H. Durrant-Whyte. Simultaneous localization and mapping (SLAM): Part II. *Robotics & Automation Magazine, IEEE 13(3),* pp. 108-117. 2006.

[21] S. Saeedi, L. Paull, M. Trentini, M. Seto and H. Li. Map merging using hough peak matching. Presented at 2012 IEEE/RSJ International Conference on Intelligent Robots and Systems (IROS), 2012.

[22] C. Estrada, J. Neira and J. D. Tardos. Hierarchical SLAM: Real-time accurate mapping of large environments. *Robotics, IEEE Transactions On 21(4),* pp. 588-596. 2005.

[23] S. B. Williams, G. Dissanayake and H. Durrant-Whyte. An efficient approach to the simultaneous localisation and mapping problem. Presented at IEEE International Conference on Robotics and Automation, 2002.

[24] J. Salvi, Y. Petillot, S. Thomas and J. Aulinas. Visual SLAM for underwater vehicles using video velocity log and natural landmarks. Presented at OCEANS, 2008.

[25] M. Montemerlo, S. Thrun, D. Koller and B. Wegbreit. FastSLAM: A factored solution to the simultaneous localization and mapping problem. Presented at In Proceedings of the AAAI National Conference on Artificial Intelligence, 2002.

[26] S. Thrun, Y. Liu, D. Koller, A. Y. Ng, Z. Ghahramani and H. Durrant-Whyte. Simultaneous localization and mapping with sparse extended information filters. *The International Journal of Robotics Research 23(7-8),* pp. 693-716. 2004.

[27] S. Barkby, S. Williams, O. Pizarro and M. Jakuba. An efficient approach to bathymetric SLAM. Presented at IEEE/RSJ International Conference on Intelligent Robots and Systems, 2009.

[28] S. Thrun and M. Montemerlo. The GraphSLAM algorithm with applications to large-scale mapping of urban structures. *INTERNATIONAL JOURNAL ON ROBOTICS RESEARCH 25(5),* pp. 403-430. 2006.

[29] G. Dissanayake, Shoudong Huang, Zhan Wang and R. Ranasinghe. A review of recent developments in simultaneous localization and mapping. Presented at 2011 6th IEEE International Conference on Industrial and Information Systems (ICIIS), 2011.

[30] H. Casarrubias-Vargas, A. Petrilli-Barceló and E. Bayro-Corrochano. EKF-SLAM and machine learning techniques for visual robot navigation. Presented at 20th International Conference on Pattern Recognition (ICPR), 2010.

[31] J. A. Castellanos, R. Martínez-cantín, J. D. Tardós and J. Neira. Robocentric map joining: Improving the consistency of EKF-SLAM. *Robotics and Autonomous Systems 55*pp. 21-29. 2007.

[32] T. Suzuki, Y. Amano and T. Hashizume. Development of a SIFT based monocular EKF-SLAM algorithm for a small unmanned aerial vehicle. Presented at 2011 Proceedings of SICE Annual Conference (SICE), 2011.

[33] A. Burguera, Y. González and G. Oliver. Underwater SLAM with robocentric trajectory using a mechanically scanned imaging sonar. Presented at 2011 IEEE/RSJ International Conference on Intelligent Robots and Systems (IROS), 2011.

[34] S. Sathyanath and F. Sahin. Application of artificial immune system based intelligent multi agent model to a mine detection problem. Presented at 2002 IEEE International Conference on Systems, Man and Cybernetics, 2002.

[35] Haihui He and Linxiang Shi. The application and research of system structure for mobile robot path planning based on multi-agent. Presented at 2010 International Conference on Computer Design and Applications (ICCDA), 2010.

[36] A. Z. Mohamed, Sang Heon Lee, M. Aziz, Hung Yao Hsu and W. M. Ferdous. A proposal on development of intelligent PSO based path planning and image based obstacle avoidance for real multi agents robotics system application. Presented at 2010 International Conference on Electronic Computer Technology (ICECT), 2010.

[37] K. Zafar, S. B. Qazi and A. R. Baig. Mine detection and route planning in military warfare using multi agent system. Presented at 30th Annual International Computer Software and Applications Conference, 2006.

[38] M. Cardoso Silva, A. C. Bicharra Garcia and A. Conci. A multi-agent system for dynamic path planning. Presented at 2010 Second Brazilian Workshop on Social Simulation (BWSS), 2010.

[39] M. Pfingsthorn, A. Birk and H. Bulow. An efficient strategy for data exchange in multi-robot mapping under underwater communication constraints. Presented at 2010 IEEE/RSJ International Conference on Intelligent Robots and Systems (IROS), 2010.

[40] Zeng Wenjing, Zhang Tie dong and Ma Yan. A novel data association approach of SLAM. Presented at 2nd International Congress on Image and Signal Processing, 2009.

[41] Yin-Tien Wang and Ying-Chieh Feng. Data association and map management for robot SLAM using local invariant features. Presented at 2013 IEEE International Conference on Mechatronics and Automation (ICMA), 2013.

[42] M. W. M. G. Dissanayake, P. Newman, S. Clark, H. F. Durrant-Whyte and M. Csorba. A solution to the simultaneous localization and map building (SLAM) problem. *Robotics and Automation, IEEE Transactions On 17(3),* pp. 229-241. 2001.

[43] J. Neira and J. D. Tardos. Data association in stochastic mapping using the joint compatibility test. *IEEE Transactions on Robotics and Automation 17(6),* pp. 890-897. 2001.

[44] M. S. T. Pohajdak, "Change detection for AUV simultaneous localization and mapping," MOOS Development and Applications Working Group, Cambridge, 2013.

[45] Bai-Fan Chen, Zi-xing Cai and Zhi-Rong Zou. A hybrid data association approach for mobile robot SLAM. Presented at 2010 International Conference on Control Automation and Systems (ICCAS), 2010.

[46] A. Gil, O. Reinoso, O. M. Mozos, C. Stachniss and W. Burgard. Improving data association in vision-based SLAM. Presented at In Proc. IEEE International Conference on Intelligent Robots and Systems (IROS), 2006.

[47] Wang Xiao-hua and Zhu Dai-xian. Efficient data association for vision-based SLAM. Presented at 2nd International Workshop on Intelligent Systems and Applications (ISA), 2010.

[48] G. Kosuru, S. Pedduri and K. M. Krishna. Data association using empty convex polygonal regions in EKF-SLAM. Presented at 2010 IEEE International Conference on Robotics and Biomimetics (ROBIO), 2010.

[49] (August, 2013). *IVER3 Autonomous Underwater Vehicle (AUV)*. Available: http://www.iver-auv.com/Iver3_AUV_Brochure.pdf.

[50] J. Fawcett, "Automated Target Recognition for Autonomous Underwater Vehicle (AUV) side scan sonar in Complex Environments," *Proc. 4th Int. Conf. and Exhibition on Underwater Acoustic Measurement,* 2011.

[51] C. Sanderson, D. Gibbins and S. Searle. On statistical approaches to target silhouette classification in difficult conditions. *Digital Signal Processing 18(3),* pp. 375-390. 2008.

[52] J. S. Sofia Suvorova, "Automated Target Recognition Using the Karhunen–Loéve Transform with Invariance," *Digital Signal Processing,* vol. 12, pp. 295-306, 2002.

[53] P. B. Chapple, D. C. Bertilone, R. S. Caprari and G. N. Newsam. Stochastic model-based processing for detection of small targets in non-gaussian natural imagery. *IEEE Transactions on Image Processing 10(4),* pp. 554-564. 2001.

[54] M. Kaess, A. Ranganathan and F. Dellaert. iSAM: Incremental smoothing and mapping. *Robotics, IEEE Transactions On 24(6),* pp. 1365-1378. 2008.

[55] J. Folkesson and H. Christensen. Graphical SLAM - a self-correcting map. Presented at 2004 IEEE International Conference on Robotics and Automation, 2004.

[56] A. Walcott-Bryant, M. Kaess, H. Johannsson and J. J. Leonard. Dynamic pose graph SLAM: Long-term mapping in low dynamic environments. Presented at 2012 IEEE/RSJ International Conference on Intelligent Robots and Systems (IROS), 2012.

[57] D. Lowe. Distinctive image features from scale-invariant keypoints. *International Journal of Computer Vision 60(2),* pp. 31-110. 2004.

[58] S. Se, D. Lowe and J. Little, "Mobile robot localization and mapping with uncertainty using scale-invariant visual landmarks," *The International Journal of Robotics Research,* vol. 21, pp. 735-758, 2002.

[59] A. C. Murillo, J. J. Guerrero and C. Sagues. SURF features for efficient robot localization with omnidirectional images. Presented at 2007 IEEE International Conference on Robotics and Automation, 2007.

[60] D. Langer and M. Hebert. Building qualitative elevation maps from side scan sonar data for autonomous underwater navigation. Presented at 1991 IEEE International Conference on Robotics and Automation, 1991.

[61] E. Coiras, Y. Petillot and D. M. Lane. Multiresolution 3-D reconstruction from side-scan sonar images. *Image Processing, IEEE Transactions On 16(2),* pp. 382-390. 2007.

[62] P. Woock. Deep-sea seafloor shape reconstruction from side-scan sonar data for AUV navigation. Presented at IEEE OCEANS, 2011.

[63] P. Woock and C. Frey. Deep-sea AUV navigation using side-scan sonar images and SLAM. Presented at IEEE OCEANS 2010.

[64] A. Burguera and G. Oliver. Intensity correction of side-scan sonar images. Presented at 2014 IEEE Emerging Technology and Factory Automation (ETFA), 2014.

[65] (December 1, 2000). *Bedford Basin, Nova Scotia: an interpretation of seabed features, materials, and processes based on geophysical and geological surveys and multibeam bathymetry*. Available: http://geogratis.gc.ca/api/en/nrcan-rncan/ess-sst/e2949a59-26bb-5901-b3f4-b559d1e45f7e.html.